Economic Geology
Vol. 74, 1979, pp. 556–589

Lithologic Determination of Mass Transfer Mechanisms of Multiple-Stage Porphyry Copper Mineralization at Butte, Montana: Vein Formation by Hypogene Leaching and Enrichment of Potassium-Silicate Protore

GEORGE H BRIMHALL, JR.

Abstract

Stoichiometric reaction coefficients of minerals and aqueous species in overall heterogeneous chemical reactions have been lithologically determined expressing intense late-stage modification of early low-grade copper-molybdenum mineralization during the growth of the large vein systems at Butte, Montana. Application of the principles of irreversible thermodynamics and conservation of mass in open chemical systems has provided the basis of a rock analysis method offering a quantitative deduction of the reaction chemistry, mass transfer, and magnitude of progressive late Main Stage hydrothermal alteration of the pre-existing mineralized wall rock. The critical information is mineral mass data derived from a systematic analysis of diamond drill core and crosscut samples from the western edge of the zone of superposition of hydrothermal events. The stoichiometric coefficient of each mineral is determined from the slope of its molar variation with Main Stage reaction progress variable, ξ, related directly to the number of moles of an index mineral used for reference. Relict chalcopyrite has been chosen in this regard as it was formed during the pre-Main Stage hydrothermal event in the area studied and has undergone progressive destruction during Main Stage activity. Stoichiometric coefficients of aqueous species are determined by charge balance and conservation of mass within the stoichiometric equations. By a conceptual removal of all severe, modifying effects caused by the large and relatively high grade Main Stage veins controlling wide and intense alteration envelopes, the nature of the early pre-Main Stage hydrothermal events have been reconstructed.

The early high-temperature (600°–700°C) mineralization consisting of fracture-controlled molybdenite and disseminated pyrite and chalcopyrite is found to be distinctly zoned in its unmodified state at the elevation of this study, approximately 3,400 feet below the surface. The early zonation in plan, from outside toward the center of the pattern, is a peripheral pyritic zone with approximately 5 weight percent pyrite, an oxide zone consisting of 1 to 2 percent magnetite plus hematite with a copper grade contributed by early chalcopyrite of 0 to 0.2 percent, and an axially symmetric maximum early chalcopyrite zone with over 0.5 percent copper surrounding a lower grade chalcopyrite interior zone with approximately 0.2 percent copper. Molybdenum grades increase continuously from essentially zero at the outer edge of the maximum early chalcopyrite zone to over 0.05 percent inside the interior low-grade early copper zone. No pre-Main Stage bornite has been recognized.

Superposition of late, relatively low temperature (200°–350°C), continuous high-grade Main Stage veins and ubiquitously related alteration envelopes upon the early disseminated sulfides and associated potassium silicate alteration has resulted in profound mineralogic effects. The earliest Main Stage modification of mineralized wall rock involves very little effect on the pre-existing pyrite and chalcopyrite, but plagioclase is converted in an outer argillic facies first to montmorillonite which in turn is replaced by kaolinite. Magnetite is partially oxidized to hematite during the early clay-forming event.

Following these incipient, Main Stage effects, more intense effects are monitored continuously by the reaction progress variable and include continuous chalcopyrite destruction and hypogene leaching of early disseminated chalcopyrite from the pre-Main Stage assemblage in the near-vein sericitic facies of alteration. Molybdenite is apparently unaffected by strong sericitization. During the early part of intense Main Stage events, total copper decreases in the rock. As the reaction continues, Main Stage fluids eventually reach saturation with respect to bornite, which precipitates in vein structures. Finally chalcocite, digenite, covellite, and enargite form in narrow high-grade veins re-

sulting in a net copper addition or hypogene enrichment. Throughout the entire span of Main Stage reaction, biotite, hematite, magnetite, orthoclase, and kaolinite after montmorillonite after plagioclase are progressively altered to an assemblage of sulfides, sericite, and quartz. Sphalerite of pre-Main Stage or early Main Stage age is slightly leached during Main Stage events.

Interpretation of the Main Stage reaction chemistry in terms of calculated phase equilibria at 250°C implies a strong pre-Main Stage mineralized wall-rock buffering effect on the hydrothermal fluids during the early stages of Main Stage reaction. With the progressive destruction of the early potassium silicate assemblage of chalcopyrite, magnetite, biotite, and orthoclase, oxidation effects proceeded, with a reduction in $a_{Fe^{++}}/a^2_{H^+}$ by three orders of magnitude, essentially at constant a_{Cu^+}/a_{H^+}. First, saturation with respect to pyrite and bornite was reached, and ultimately high-grade chalcocite, covellite, enargite assemblages formed during the most intense sericitization of the wall rock at values of ξ greater than 0.5. The presence of early pre-Main Stage chalcopyrite is interpreted to be of primary importance in buffering the initial Main Stage fluid composition at a relatively high value of log a_{Cu^+}/a_{H^+} near −4.5 causing subsequent hypogene sulfide saturation in the high-grade veins.

Although the approach taken is admittedly macroscopic in nature in that the physical details of diffusion and infiltration are not considered, it has been possible to analyze exceedingly complex rock masses and to understand the coupling of mineralization and alteration, revealing the importance of element recycling to the vein-forming process. It is possible that much of the element content, i.e., base metals and sulfur, of high-grade Main Stage Butte veins originated as disseminated sulfides in the early hydrothermal protore mass which underwent a progressive hypogene redistribution and enrichment during a late-stage fracture-fluid circulation event possibly related to cooling porphyry intrusives that were emplaced after and geometrically offset from the earlier pre-Main Stage intrusives and hydrothermal events.

Introduction

THE spatial distribution of individual minerals in the ore deposit at Butte, Montana, represents an outstanding example of complex ore zonation developed by progressive superposition of hydrothermal events, each with a distinct structural control. Relatively young, high-grade vein structures with enormous lateral and vertical continuity span much of the district, overlapping, in the central portions, an early subsurface low-grade mass composed of fracture-controlled molybdenite and disseminated pyrite and chalcopyrite (Sales, 1913; Meyer, 1965; Meyer et al., 1968; Miller, 1973; Brimhall, 1977). Although previous investigations have treated the individual ore-forming events, termed the Main Stage and pre-Main Stage, respectively, an important problem remains of understanding the combined effects of both stages of mineralization and wall-rock alteration produced by circulation of magmatically heated hydrothermal fluids.

In the zone of overlap of Main Stage and pre-Main Stage events, combined mineralogic effects result in a complex ore mass. A given volume of rock may bear the effects of each successive and often dissimilar hydrothermal event, and, in this regard, the ultimate mineral assemblage and metal grades at any point in space are a unique consequence of both continual and episodic chemical interaction of hydrothermal fluid and pre-existing mineralization. Conceivably there are numerous types of possible interaction depending upon a wide variety of geologic conditions, including the chemical composition of the Main Stage fluids, the extent of Main Stage reaction, and the mineralogy of the pre-Main Stage assemblage at a given point in space, pressure, and temperature. As an example of one possible interaction type, consider the physical transfer of material, e.g., copper, from one ore mineral assemblage to another younger assemblage by the introduction of hydrothermal fluids. Initially copper is present as disseminated chalcopyrite within a dense network of pre-Main Stage alteration envelopes, but with Main Stage fracture development and circulation of lower temperature aqueous fluids, the chalcopyrite may be out of equilibrium with respect to the newly imposed surroundings and undergo replacement or dissolution as the high-grade veins form. Geologic processes of this type may be exceedingly dependent upon the previous history of the fluid and rock as well. Examples of path dependency appear to be commonplace in hydrothermal systems in which infiltrative fluid migration occurs through a dense interconnecting network of fractures and faults exposing extensive reactive surfaces to circulating fluids. Initial chemical interchange between fluid and surrounding fresh country rock or previously fractured, altered, and mineralized wall rock takes place at the new fracture surface-fluid interface and migrates progressively outward producing alteration

envelopes involving diffusional mechanisms (Meyer et al., 1968). The exact relationship of this wall-rock alteration to economic mineralization has been a basic problem in hydrothermal ore genesis as geologic complexity due to superposition and interaction of sequential events has often obscured the evidence necessary to ascertain the sources of ore-forming components as well as the critical mechanisms of vein and disseminated ore deposition operative at various times during the growth of the deposit.

Although stable isotope geochemistry has made it possible to determine the dominant source of water in the Main Stage as being meteoric (Taylor, 1974), the source of the metals remains uncertain. Remobilization and redeposition of pre-Main Stage metals as well as introduction of new chemical elements, either through Main Stage magmatic sources or by alteration stripping of trace elements from previously unaffected wall-rock minerals, are all possible mechanisms warranting close analysis. As much of the Butte district is as yet unexplored, it is impossible at this time to assess quantitatively the exact level of element remobilization during multiple mineralization events in the deposit as a whole. Nevertheless, it is quite possible to determine quantitatively the local chemical mechanisms of mass transfer by which late fluids interact with previously mineralized wall rock and thereby indirectly infer the source of metals in the high-grade Main Stage veins. Fortunately, in this regard the homogeneous composition of the Butte Quartz Monzonite wall rock reduces the number of parameters affecting the resultant fluid-rock interaction. The Butte deposit is therefore an excellent environment in which to study the effects of irreversible mass transfer.

As in mining districts around the world, continued extraction of high-grade, relatively near surface, deposits eventually depletes economic ore reserves necessitating exploration and definition of new metal resources at depth. Although underground selective Main Stage vein mining at Butte has lasted for over a century, mining activity has recently shifted toward higher productivity methods requiring complete removal of enormous tonnages of low-grade material (Miller, 1973). The geological staff of the Anaconda Company's Butte operations is actively engaged in an extensive deep underground exploration program directed at discovering and developing large tonnages of ore containing metal contributions of both the Main Stage and pre-Main Stage events. Initial formulation of the problems treated in this paper grew out of the ongoing underground exploration program at Butte in an attempt to understand the complexly zoned multiple-stage copper-molybdenum-silver mineralization.

Previous Work

Inasmuch as most successful mineral exploration is largely based upon some type of conceptual genetic model, recent studies have greatly contributed to the productive search for porphyry copper deposits which may collectively account for 85 percent of the recognized copper reserves of the Western Hemisphere, and 62 percent of the known reserves of the world (Sutulov, 1974). A generalized descriptive model of the lateral and vertical zonation of porphyry copper mineralization and alteration (Lowell and Guilbert, 1970) has been proposed and widely used in exploration for large-scale target definition by directly comparing available exposures in a given district with the zonation patterns of the generalized model. Detailed descriptions of individual deposits have immeasurably improved the interpretation of the space-time patterns and relations of the mineralization, alteration, volcanism, intrusion, and fluid composition allowing well-documented reconstruction of the physical environments of deposition (Gustafson and Hunt, 1975; Wallace et al., 1968; Meyer et al., 1968; Barton et al., 1977). Normal crustal processes involving lithospheric plate motion, subduction, and magma generation near Benioff zones, and ultimate ascent of calc-alkaline host intrusives (Sillitoe, 1972), offer a possible, yet speculative, indication of potential regional controls on host magma localization in some areas such as the South American Cordillera. Smaller scale mechanisms which may be important in the generation and ultimate concentration and transport of ore-forming components have been studied both theoretically and experimentally including the formation of fractures around intrusions (Koide and Bhattacharji, 1975), vapor generation in silicate melts (Burnham, 1967; Whitney, 1975), generation of metal-chloride complexes (Kilinc and Burnham, 1972), fluid composition variations (Roedder, 1971), influx of meteoric water (Taylor, 1974), and groundwater convection near cooling intrusives (Cathles, 1977; Norton and Knight, 1977; Norton and Knapp, 1977).

Although metal concentration in hydrothermal fluids and aqueous transport processes are important in the ore-forming process as a whole, it is necessary to understand better the processes which are ultimately responsible for sulfide deposition. Several sulfide precipitation mechanisms have been proposed which are based upon the experimentally determined variation of sulfide solubilities with temperature, salinity, and pH (Crerar and Barnes, 1976). It has been shown that temperature gradients alone probably cannot account for ore localization and that wall-rock alteration reactions, salinity gradients, or boiling are necessary to explain the observed metal concen-

trations within ore zones (Cathles, 1977). Genetic and spatial association of hydrothermally altered wall rocks and fracture-controlled sulfides are quite common (Meyer and Hemley, 1967; Meyer et al., 1968; Brimhall, 1977), indicating the importance of irreversible reactions between ore-forming solutions and surrounding wall rock to the final deposition of sulfides. Helgeson et al. (1969) have examined the implications of irreversible hydrothermal rock alteration in idealized computer simulations of ore deposition and have shown sulfide saturation to be in part related to changing activity of hydrogen ion produced by silicate reactions. The thermodynamic and kinetic principles involved in theoretically simulating geochemical systems has been established with exceptional rigor (Helgeson, 1968; Helgeson et al., 1969; 1970; Helgeson, 1971). From these studies emerges a basic conceptual tool in the form of sequential mineral asesmblages and solution composition reaction paths predicted for the simulated interaction of a specified rock and solution composition (Helgeson et al., 1969; Helgeson, 1970; Villas and Norton, 1977; Knight, 1977).

Approach

Although the basic principles exist which are necessary to predict complex path-dependent behavior in simulated hydrothermal systems, more research of a petrologic nature is necessary to ascertain the dominant geologic controls on repetitive concentration of metals. In this paper a new and general lithologic approach is developed for the analysis of the interdependence of wall-rock alteration and ore deposition during successive mineralization events. Quantitative measurements of actual mass transfer due to aqueous metasomatism and irreversible chemical reaction are deduced from geological data derived by routine detailed mapping of diamond drill core and underground exposures coupled with laboratory mineral mass determinations. Basic to the method is an accurate characterization of an entire composite ore mass composed of a large number of component geologic units which are described accurately in terms of rock types, wall-rock alteration, abundance, and orientation of various vein stages, mineralogy of ore phases, and the base metal contribution of each sulfide to the total metal grade of the sample. A major attribute of the method is the ability to contend with rock masses generated by successive hydrothermal events, eliminating the necessity to rely upon fortuitously preserved specimens formed by single-stage events.

General Geology of the Butte District

For more than a century the Butte district has been famous for its extensive vein mineralization and

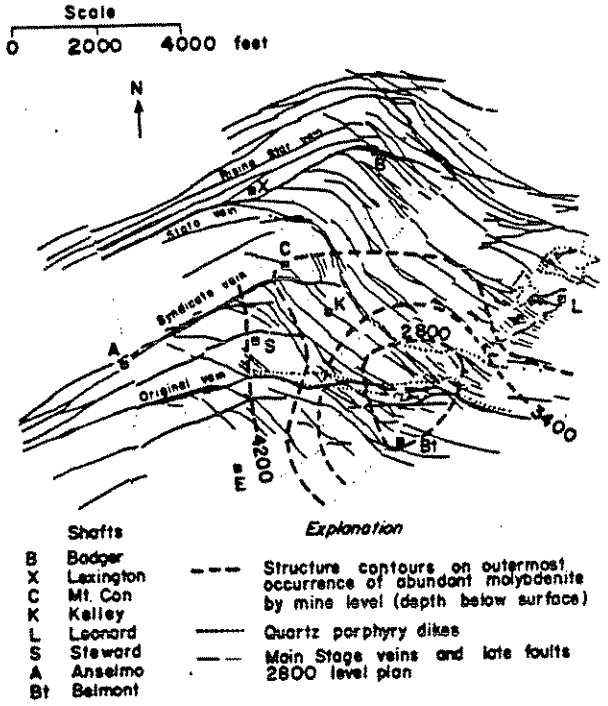

FIG. 1. Plan map of Butte district, Montana, showing the locus of pre-Main Stage occurrences of abundant molybdenite by structure contours given by mine level, approximately equal to the distance below the surface. Two ages of quartz porphyry intrusives are shown. The earliest east-west Steward dikes span the length of the molybdenite dome structure with the northern dike striking to the northwest toward the Kelley shaft. The younger Modoc quartz porphyry masses are near the Leonard shaft, north of the Steward quartz porphyry system. Main Stage Butte veins are shown on the 2,800 level overlapping the molybdenite dome in a circular area just north of the Belmont shaft. The zone of pre-Main Stage and Main Stage overlap widens downward, as the structure contours on the molybdenite dome expand outward.

called the "Richest Hill on Earth." The deposit is in the south end of the Boulder batholith, a composite monzonitic intrusive in which the dominant rock type is the 70 to 72 million-year-old Butte Quartz Monzonite. Narrow east-west striking quartz porphyry dikes intrude the Butte Quartz Monzonite. Often associated with the contacts of these "Steward-type" quartz porphyry dikes and surrounding Butte Quartz Monzonite are narrow breccia zones containing wall-rock fragments in a matrix of alkali feldspar, biotite, quartz, and disseminated pyrite and chalcopyrite, representing the first megascopically visible introduction of copper into the district (Brimhall, 1973, 1976, 1977; Miller, 1973). In the deeper portions of the Butte district, crosscutting both the Butte Quartz Monzonite and Steward quartz porphyry dikes are abundant, narrow, and discontinuous veinlets controlling alteration halos characterized by the presence of fine-grained secondary alkali feldspar, with vari-

able amounts of quartz, muscovite, biotite, anhydrite, and magnetite. Disseminated pyrite and chalcopyrite occur within these alteration envelopes, formed at temperatures in the range of 650° ± 100°C based upon alkali partitioning between coexisting feldspar and muscovite (Brimhall, 1977). Crosscutting the alkali feldspar stable veins and alteration assemblages which are apparently about 62 to 63 million years old are somewhat younger quartz or quartz molybdenite veins without intense alteration halos, which in some cases are relatively continuous and are rebroken during later hydrothermal events (Proffett, 1973). The distribution of molybdenite-bearing quartz veins is shown in Figure 1 in plan by structure contours of equal elevation given as depth below surface. Occurrence of abundant molybdenite is restricted to the interior of a dome-shaped subsurface volume (Meyer et al., 1968) in the Butte district with closure on the 2800 level expanding downward. The north-south striking Continental fault, with substantial vertical displacement, has upfaulted the deep molybdenite-bearing monzonite at the eastern end of the district so that surface exposures exhibit molybdenite occurrences and often andalusite in addition to other pre-Main Stage minerals (Brimhall, 1977). Much of the earlier disseminated pyrite-chalcopyrite occurrences are within the molybdenite dome. Pervasive biotitization of igneous hornblende has been affected by all early veins (Roberts, 1973).

Consistently crosscutting the early fractures are much larger and more continuous high-grade vein structures, formed at lower temperatures, controlling intense sericitic alteration halos adjacent to the veins which yield outward to an argillic halo composed of an inner kaolinite and outer montmorillonite subzone (Meyer et al., 1968). The 57 to 59 million-year-old Main Stage structures are shown in Figure 1 on the 2800 level with important shafts for reference. The earliest Main Stage veins in the district, called the Anaconda system, strike roughly N 65° E, dip steeply, and have individual ore shoots thousands of feet long and 20 to 30 feet wide. These veins are faulted and offset by southwest-dipping, northwest-striking veins, called the Blue system, with average widths of about 5 to 20 feet. These veins are best developed in deep levels of the western portion of the district and are relatively narrow and low grade near the surface. The youngest Main Stage structures, the Hanging Wall Steward veins, occur only in the deep levels of the district between the Steward and Belmont mines and strike east-west with flat southerly dips (Proffett, 1973). Zones of closely spaced Main Stage mineralized fractures, called Horsetail structures, exist between the Leonard and Belmont shafts. Cut by these horsetail structures are quartz porphyry dikes of the Modoc system which becomes pluglike at depth in the Leonard mine. These intrusives are younger than the east-west-striking quartz porphyry dikes near the Steward and Kelley shafts (Steward type), as associated breccias contain rock fragments with pre-Main Stage quartz molybdenite veins (S. A. Roberts, pers. commun.).

Mineralization in the large Main Stage veins is arranged in crudely concentric zones of zinc and manganese around a central zone of copper (Meyer et al., 1968). Local terminology describes the zonation as a central zone in which veins are free of sphalerite, an intermediate zone in which ores are predominantly copper but often have some sphalerite, and a peripheral zone of sphalerite veins. Within the zone of overlap of Main Stage veins and pre-Main Stage events shown by the molybdenite dome in Figure 1, the major veins are mineralogically zoned. In the upper levels, above the 2800 level, pyrite, bornite, enargite, and chalcocite are the common vein minerals, yielding downward to pyrite, chalcopyrite, and bornite. In an easterly direction, the Main Stage sulfides become pyrite, chalcocite, covellite, and enargite.

Physical conditions during Main Stage activity were vastly different than during the high-temperature pre-Main Stage events. Fluid inclusion data imply a Main Stage temperature range for the whole deposit of 200° to 350°C with the peripheral zone not more than 50 degrees cooler than the central zone (Meyer et al., 1968). Further evidence substantiating the maximum 350°C temperature of Main Stage activity comes from K-Ar dating of igneous biotite in Butte Quartz Monzonite adjacent to Main Stage halos. Radiogenic argon was retained by these biotites during the Main Stage event and their apparent ages were not reset, implying maximum Main Stage temperatures of less than the presumed argon retention temperature of 350°C (P. Damon, in prep.).

In any volume of Butte Quartz Monzonite with pre-Main Stage as well as Main Stage effects present, there is an apparent gap in the sequence of hydrothermal events represented by an early high-temperature assemblage and a much lower temperature assemblage approximately 5 m.y. younger. It is unlikely that this interval represents a prolonged evolution at a single hydrothermal event caused by a cooling magma at depth. The Modoc dike system offers a possible explanation for this prolonged interval by providing a possible heat source of intermediate age which may have, at least in part, been responsible for Main Stage fluid circulation and perhaps introduction of elements. The ultimate source of the metals, sulfur, and arsenic in the Main Stage vein structures is a problem of basic concern.

General Geological Considerations

Within the porphyry base metal environment it is possible for the locus of hydrothermal mineralization to shift spatially as a consequence of changes in the thermal regime causing fluid circulation. Conceivably the migration of zones in which active fluid-rock interaction occurs may in part be due to the thermal collapse of individual circulation cells utilizing a given fracture system or may result from multiple igneous intrusion (Wallace et al., 1968; Gustafson and Hunt, 1975) or the generation of a new network of channelways controlling a new flow pattern. Successful exploration for large and complex targets formed during progressive hydrothermal activity is exceedingly expensive and requires clear understanding of the position and zonation of individual ore zones. It is possible that simple superposition of hydrothermal effects is not strictly additive in that relatively young hydrothermal episodes may remobilize base metals in previously formed mineralized zones resulting in a depletion in the total metal content of the rock. Formulation of optimum exploration targets is therefore complicated conceptually as the highest total metal grades may not necessarily be located in the zones of overlap of two or more events. In order to ascertain the zonation of a given event at the time of formation, it is necessary to determine and remove the effects of subsequent fluid-rock interaction including the introduction, remobilization, and reprecipitation of metals.

The geometry of fracture systems controlling fluid-rock interaction determines the ease with which mineral assemblages can be unambiguously ascribed to a particular hydrothermal event. In the simplest case, one can imagine that the veins and alteration envelopes superimposed upon an early ore zone are widely spaced, leaving islands of the early ore type unaffected. In this ideal, yet rare, instance the character of the early mineralization upon which Main Stage effects were superimposed is readily discernable. As the degree of Main Stage alteration halo overlap increases in a zone with high vein density, it would seem that deduction of the nature of pre-existing ores would become impossible by megascopic analyses.

The superposition of Butte Main Stage veins and intense alteration facies upon the early pre-Main Stage zonation (Brimhall, 1976) seems to be analogous to the collapse and encroachment of fluids causing late pyrite veins with sericite and hypogene clay alteration upon early central potassium silicate core zones containing chalcopyrite and bornite in the porphyry copper environment as a whole (Taylor, 1974). Considering the geometrical volume with macroscopic dimensions of multistage economic ore zones as chemical systems, produced in part by convective circulation of magmatic and/or meteoric water, it is clear that, relative to the composition of average crustal rocks, base metal introduction occurred within the boundaries of the system. The mineralized zones are then open or metasomatic chemical systems in that material transfer takes place across their boundaries. Furthermore, the ore zones represent reactive chemical systems in which mass transfer occurs in part by chemical reaction due to an imposed disequilibrium of rock and fluid.

Irreversible Chemical Thermodynamics of Open Chemical Systems

Several geologic environments that are responsible for severe modification of ore masses by metasomatism and chemical reaction have been discussed in the literature, for example, the processes of supergene leaching and secondary enrichment in chalcocite blankets (Anderson, 1955). The mechanisms of metal transfer are generally understood as being part of surficial weathering phenomena that may occur over a substantial interval of geologic time during which climate and ground-water hydrology exert important influences on the ore mass. By analogy with these low-temperature supergene effects it should be possible to understand progressive modification of early ore masses in the deep-seated hypogene environment. Processes of hypogene ore modification may be deduced from careful analysis of the observed mineralogic effects and represented in a temporal framework utilizing the available geologic clocks. Relative structural and "absolute" radiometric criteria have been discussed which offer discrete ages of events. Another type, and perhaps more useful geochronometer in this context, will be discussed which offers the type of continuous monitoring of mineralogic change necessary to formulate the principles of hypogene ore modification. This measure of progress is based upon conservation of mass in open chemical systems and offers a quantitative means of analyzing the effects of fluid introduction into fractures including the coupling of mineralization and alteration. The effects caused by late-stage hydrothermal migration are analyzed in terms of a suite of geological samples each considered as an open chemical system having undergone various levels of modification. For normal radiometric dating methods, complex alteration is often a serious hindrance. We will show that by use of a chemical mass balance clock these same alteration features, in contrast, become very useful measures of reaction progress.

Conservation of mass during heterogeneous chemical reaction

In an open chemical system involving fluid motion, mass and energy may be exchanged through the boundaries, but there must be an overall conservation of mass and energy as a whole. If enrichment of ore metals occurs within the system, a depletion of those metals must occur outside the system. The change in mass of species, i, within an open system may be divided into an external part, $dm_{i,ext}$ supplied from outside the system, and an internal part, $dm_{i,int}$ due to changes within the system resulting from chemical reaction (Prigogine, 1955).

$$dm_{i,total} = dm_{i,ext} + dm_{i,int} \quad (1)$$

Change in mass due strictly to a single chemical reaction may occur over the duration of the process. Using the degree of advancement or extent of reaction, ξ, with units of moles introduced by De Donder (1928, 1936), it is possible to express the change in mass during a given reaction as equation (2) representing the internal change in mass of a system, in which M_i is the molecular weight of species i. As a reaction proceeds, ξ increases from zero at the start and continuously monitors the unidirectional progress of the reaction.

$$dm_{i,int} = \nu_i M_i d\xi \quad (2)$$

The coefficients (ν_i), designated by small letters in (3), are stoichiometric reaction coefficient for each species, i, taking part in the reaction. A stoichiometric coefficient is counted as positive when a species, i, appears as a product on the right-hand side of the equation and negative when species i is a reactant. For example, consider a heterogeneous reaction between solid mineral species A and B and a fluid phase containing aqueous species C and D producing a new mineral species E and gaseous species F. Even in an open system in which mass is either introduced or extracted, in this example by the reacting fluid, the overall reaction may be written as (3).

$$aA + bB + cC_{aqueous} + dD_{aqueous} \rightarrow eE + fF_{gas} \quad (3)$$

Combining (1) and (2) gives (4), an expression for the total change in mass of species i in a system involving a single chemical reaction and mass exchange with the surroundings.

$$dm_{i,total} = dm_{i,ext} + \nu_i M_i d\xi \quad (4)$$

Simultaneous reactions may be treated in a similar manner and the total change in mass of species i is given in (5) summed over all chemical reactions, $\rho = 1$ to r.

$$dm_{i,total} = dm_{i,ext} + M_i \sum_{\rho=1}^{r} \nu_{i,\rho} d\xi_\rho \quad (5)$$

Instead of the mass transfer of a species it is useful to consider the mole transfer which may be derived by dividing equation (5) by the molecular weight, M_i, of species i. Equation (6) is a very useful formula relating externally and internally produced changes in moles, n_i, within a chemical system.

$$dn_{i,total} = dn_{i,ext} + \sum_{\rho=1}^{r} \nu_{i,\rho} d\xi_\rho \quad (6)$$

The equations outlined indicate which thermodynamic parameters are critical for an analysis of chemical interaction and mass transfer in an open geochemical system from a lithologic standpoint. Considerations of conservation of mass (6) offer the most practical solution to the problem. The relative masses or moles of minerals in a rock provide us with a splendid documentation of mass transport between rocks and fluids ultimately manifested in commonly used and economically important parameters such as copper grade.

In practice a single index reactant mineral is chosen, e.g., chalcopyrite which is present in the pre-Main Stage or early ore assemblage which undergoes modification by Main Stage fluids. The size of the chemical system is defined such that the stoichiometric coefficient of the index mineral is 1.0 and that there is 1.0 moles of index mineral at the start of the reaction when $\xi_\rho = 0$. This formulation requires that we know the initial chalcopyrite concentration before late-stage modification begins. A simple and accurate method will be shown to deduce the early chalcopyrite content in a subsequent part of this paper. The stoichiometric reaction coefficients of all other species may be derived using modifications of equation (6). Instead of considering each of the simultaneous reactions, $\rho = 1$ to r, we will be concerned with the net chemical reaction responsible for mineralogic change in the system including both wall-rock alteration and sulfide deposition or replacement. Equation (6) is greatly simplified by this approach. An overall progress variable, $\bar{\xi}$, is used to express the extent of the net reaction, and the stoichiometric coefficients, $\nu_{i,\phi}$, apply to the overall progress variable, (7), and to the particular net reaction, ϕ, occurring over a given interval of $\bar{\xi}$.

$$dn_{i,total} = dn_{i,ext} + \nu_{i,\phi} d\bar{\xi} \quad (7)$$

Upon dividing (7) by $d\bar{\xi}$, an expression for the stoichiometric coefficients emerges, (8).

$$\frac{dn_{i,total}}{d\bar{\xi}} = \frac{dn_{i,ext}}{d\bar{\xi}} + \nu_{i,\phi} \tag{8}$$

Determination of stoichiometric reaction coefficients from mineralogical data

The mole transfer with respect to the external part of the chemical system takes place only through the exchange of aqueous species with the hydrothermal fluid. Consequently, no solid species or minerals physically move in or out of the system, requiring that the second term in (8), $dn_{i,ext}/d\bar{\xi}$, be equal to zero for minerals, resulting in (9) for the net chemical reaction affecting mineralogic change.

$$\frac{dn_{i,mineral}}{d\bar{\xi}} = \nu_{i,\phi} \tag{9}$$

This equation has very fundamental geologic significance as it relates the moles of mineral species in a rock to an overall chemical reaction expressing quantitatively the heterogeneous reaction stoichiometry and casts both the mineralogy and chemistry in a relative temporal framework. The stoichiometric coefficients of the mineral species, $\nu_{i,\phi}$, may be determined by calculating the first derivative of n_i with respect to $\bar{\xi}$. It is therefore necessary to deduce an expression for the reaction progress variable, $\bar{\xi}$.

Determination of reaction progress variable, $\bar{\xi}$

The reaction progress variable, $\bar{\xi}$, may be determined in a physically meaningful form by first expressing (9) as (10).

$$dn_{i,minerals} = \nu_{i,\phi} d\bar{\xi} \tag{10}$$

This expression may be integrated for any mineral species, i, but for simplicity we will consider only the reactant index mineral, i = I, as shown in equation (11).

$$n_I - n^0_I = \nu_{I,\phi}(\bar{\xi} - \bar{\xi}^0) \tag{11}$$

Superscripted quantities n^0_I and $\bar{\xi}^0$ refer to initial states. As mentioned previously, the index mineral chosen is chalcopyrite and $n^0_I = 1.0$, $\nu_{I,\phi} = -1.0$, $\bar{\xi}^0 = 0.0$.

Upon substitution of these, (11) becomes (12)

$$n_{chalcopyrite} - 1 = -\bar{\xi} \tag{12}$$

which may be rewritten as (13) giving an expression of the reaction progress variable in terms of the number of moles of chalcopyrite present in a rock, a quantity easily determined physically.

$$\bar{\xi} = 1 - n_{chalcopyrite} \tag{13}$$

Stoichiometric coefficients of the aqueous and gaseous species in an overall net reaction may be determined by first deducing the coefficients of the minerals by rock analysis and then balancing the resulting reactions on charge and mass. The internal and external components of mass or mole balance are thereby represented in heterogeneous chemical reactions involving minerals and mobile species in the fluid phase. The exact speciation of the aqueous phase is not important in expressing the mole transfer in the system, but if necessary may be estimated from experimental data or theoretical calculation (Crerar and Barnes, 1976). The actual processes of ore deposition and wall-rock alteration may be expressed by net chemical reactions and temporally arranged by use of the extent of reaction or reaction differential, $d\bar{\xi}$, which, although it does not offer absolute age information, provides a chemically more useful measure of geologic progression during a discrete interval of time. This mass balance clock provides a monatonic sequential scale of hydrothermal effects which may have occurred simultaneously, but at various levels of intensity, in different places. A remarkable magnification of the scale of geologic deduction results, offering a new level of comprehension of physical process.

Rock Analysis Methods

Although thermodynamic relations indicate a straightforward method of determining lithologically irreversible mass transfer relations through the use of the overall progress variable, $\bar{\xi}$, geological reality introduces a significant element of complexity which is not fully apparent in the equations. In practice, analysis of multistage mineralization and alteration requires a knowledge of the characteristic mineral assemblages of the various events which is obtained only through careful field mapping and petrography (Meyer, 1965; Guilbert and Zeihen, 1964). This includes an integrated consideration of wall-rock types, intrusives, alteration assemblages, abundance, orientation, and nature of veins and sulfide disseminations, faults, ore mineralogy, relative ages of structures, and assay values for a number of chemical elements.

Collection of the critical mineral mass data in a temporal context may be accomplished by detailed mapping of megascopically visible geological features, e.g., alteration, veins, and rock types, coupled with quantitative microscopic determination of the ore mineral assemblage and mass of each mineral phase using representative splits of drill core assay pulps or crosscut channel samples which have been subjected to heavy mineral separation. Alternatively, whole-rock chemical analyses or powder diffractometry may be used to deduce the mineralogy, but modal ambiguities and large errors may result due to the multi-

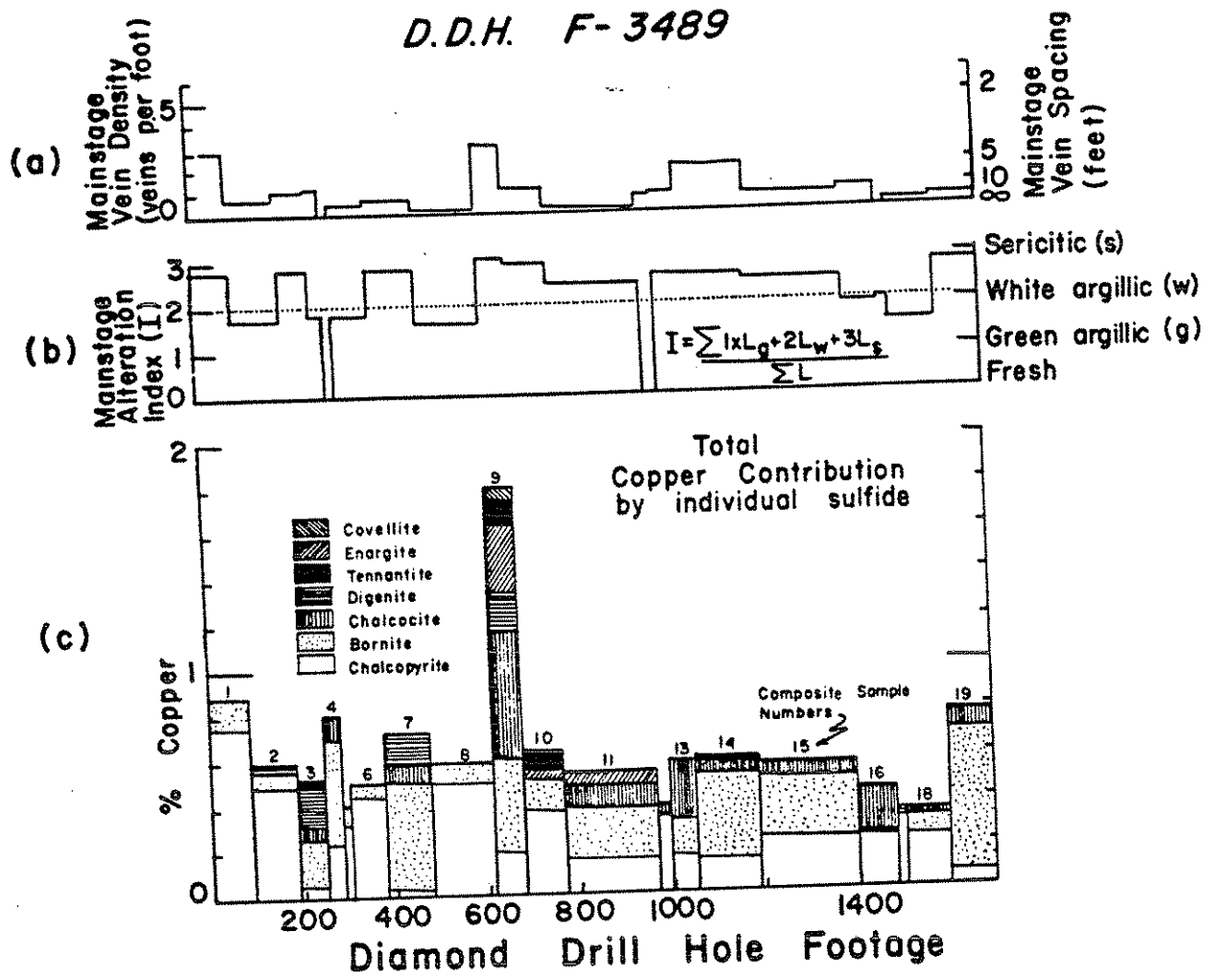

FIG. 2. Representative diamond drill hole penetration through multiple-stage mineralization (D.D.H. F-3489) drilled nearly flat (−5°) with a northeast (N 50° E) trend. Location shown on Figure 6; collar position is in F-3483 crosscut south.

Figure 2a illustrates the variation of Main Stage vein density (veins per foot) with distance down the diamond drill hole, as defined over composite lengths using detailed core logging on a scale of 1 inch = 20 feet. Figure 2b presents the variation in Main Stage alteration facies intensity with drill hole distance using alteration index as a length (L) weighted parameter with sericitic (most intense) arbitrarily assigned a value of 3, white argillic (kaolinite) as 2, green argillic (montmorillonite) as 1, and fresh Butte Quartz Monzonite (with pre-Main Stage effects) as 0. Notice the excellent correlation between Main Stage vein density and overall alteration index. Figure 2c presents the total copper variation with drill hole distance as well as the contribution to the total copper grade by each sulfide: covellite, enargite, tennantite, digenite, chalcocite, bornite, and chalcopyrite. Composite sample numbers 1 to 19 are assigned consecutively from drill hole collar to end of hole throughout this paper. High-grade zones with high Main Stage vein density and high alteration index generally have relatively low chalcopyrite contribution to overall copper grade.

plicity of mineral phases present. It is important to assess quantitatively the amounts of even minor phases, such as chalcocite, as relatively large copper contributions may be involved, requiring application of the most accurate available mineral counting method.

Rigorous geochemical documentation of metallogenic events is possible only through a unification of all these data. To be of optimum value and to gain necessary support both in a research and exploration framework, the geological data should not only provide the necessary lithologic basis for a detailed scientific analysis of the geologic events but, in addition, should supply pertinent information to mine planning groups, including a detailed and exceedingly accurate mineral inventory which contains rock mechanical

properties of the ore mass (Pillar and Drummond, 1975) and mineralogic data applicable to process metallurgical control (Petruk, 1976). Furthermore the unified information must be readily accessible if it is to be of any use in the solution of either practical or academic problems. Excellent geological data retrieval systems are available and are in use in exploration (Ekström et al., 1975). The method developed in this paper provides considerable flexibility in the application of geologic and mineralogic data to a wide variety of problems. Especially useful in exploration is the capability of determining the separate zonation and directional gradients of individual metallogenic parameters allowing definition of complex targets of optimum metal grade and tonnage.

Field methods

Of all the data necessary to determine the physical controls upon hydrothermal ore deposition, geologic mapping is by far the most critical as the sequence and characteristic mineral assemblages of single metallogenic events are revealed only by careful observation of the causative fractures and representation in a geometrical and temporal framework (Wallace et al., 1968; Meyer et al., 1968; Miller, 1973; Proffett, 1973; Brimhall, 1973). Mapping of diamond drill core and underground exposures on a scale of 1 inch to 20 feet has provided the necessary geological data in Butte. Lithologic boundaries, such as rock-type contacts or changes in the alteration facies recognized by mapping, provide convenient and meaningful breaks on which to subdivide composited samples which are subsequently crushed, pulverized, assayed, and subjected to laboratory analysis.

Laboratory methods and computer calculation

The accuracy of modal data has been substantially improved by separation of the component minerals into individual groups utilizing differential mineral density. A study has been made in order to discover a reliable method of heavy and light mineral analysis specifically designed to determine feasible methods of grain separation, epoxy block impregnation of the separates, and optimal mineral counting procedures yielding accurate results even for minor phases. The optimal method found, and the one used in this study, is described in the Appendix, including a discussion of the routine procedures used in exploration and laboratory data collection, coding, and computer calculation.

Graphical determination of initial pre-Main Stage copper contribution

As mentioned previously, we will utilize chalcopyrite as an index mineral and depending upon the quantity present in each sample comprising a suite, determine ξ and the stoichiometric coefficient of each mineral. It is therefore necessary to determine the original concentration of chalcopyrite in the pre-Main Stage assemblage before later hydrothermal alteration occurred.

Superimposed mineralization of the Butte Quartz Monzonite as well as mineralization of a number of relatively infrequent wall-rock types such as quartz porphyry intrusive results in a heterogeneous spacial distribution of copper. The variability of metal grades is of course a function of the size of sampling interval. Main Stage veins tend to be much higher grade than the interveining pre-Main Stage alteration envelopes containing disseminated chalcopyrite, although the latter may contain up to 2 percent copper. Main Stage structures often occur in parallel sets. Consequently it is useful to express the relative frequency of these structures by the Main Stage vein density in a given direction, for example along a diamond drill hole. Figure 2 presents a graphical correlation of Main Stage vein density, alteration index, and total percent copper (Main Stage plus pre-Main Stage) as functions of distance in a relatively flat diamond drill hole on the 3400 level. Intervals characterized by high Main Stage vein density and sericitic alteration usually are relatively high grade and contain a high copper contribution by one or more of the following sulfides which have been accurately identified (see Appendix): chalcocite, bornite, digenite, tennantite, enargite, and covellite, with very little chalcopyrite. Obviously, for our purposes the age of chalcopyrite is of upmost importance. Fortunately, at this elevation on the western side of the Butte district, the Main Stage veins are characterized by pyrite, enargite, bornite, and chalcocite. Directly below, however, on deep mine levels the veins contain pyrite, chalcopyrite, and bornite as the dominant sulfides (Meyer et al., 1968). Recent petrographic studies of polished slabs show that, although chalcopyrite occurs in Main Stage veins on the deep levels, it is very rarely present in high-grade Main Stage veins on the upper levels and is definitely the only pre-Main Stage copper-bearing sulfide. The apparent inverse relationship between the copper contribution of chalcopyrite in Figure 2 and that of other sulfides characteristic of the Main Stage at the 3400 level implies a Main Stage modification effect of pre-existing chalcopyrite, which is most severe in zones with a high Main Stage vein density and high alteration index.

A graphical method has been derived which depicts the magnitude and nature of the Main Stage modification of pre-Main Stage pyrite-chalcopyrite-molybdenite-magnetite-hematite assemblages. Individual composite samples are represented by a plot of percent total copper determined by atomic absorption

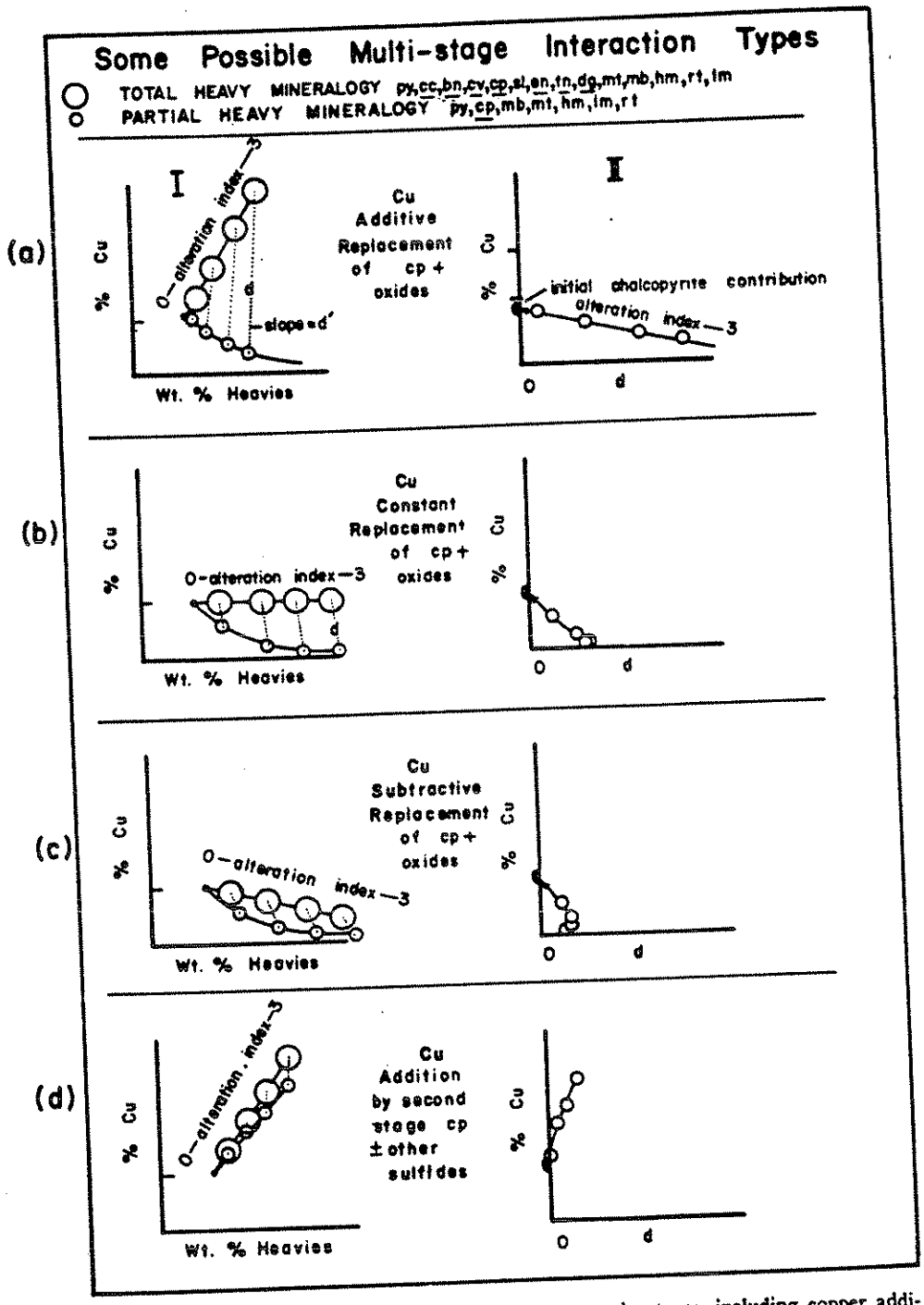

FIG. 3. Graphical representation of possible Main Stage reaction types, including copper additive replacement of the pre-Main Stage assemblage (a), copper constant replacement (b), copper subtractive replacement (c), and Main Stage vein formation with chalcopyrite (d). Alteration index increases with high values of d.

versus total weight percent heavy minerals determined gravimetrically (Fig. 3a-I). For each composite a corresponding point, found by calculation, is plotted for the percent copper contribution due only to chalcopyrite and the partial weight percent heavy minerals due only to pyrite, chalcopyrite, magnetite, molybdenite, and hematite. Each composite is then depicted by a tie line relating present total-rock

values (Main Stage plus pre-Main Stage) to relict pre-Main Stage content including, of course, some Main Stage pyrite. The tie line is represented in two-dimensional vector space as $\vec{d}$, and the absolute value or length of $\vec{d}$ is calculated from its two orthogonal components (14) for a given sample.

$$|d| = [(W_T - W_P)^2 + (G_T - G_P)^2]^1 \quad (14)$$

W_T is the total weight percent of all heavy minerals in the sample with specific gravity greater than 3.31. W_P is the partial heavy mineral content in weight percent of the characteristic pre-Main Stage assemblage plus additional Main Stage pyrite. G_T is the total whole-rock copper grade, and G_P is the copper grade due only to chalcopyrite.

The magnitude of $\vec{d}$ is used in Figure 3a-II as the independent variable in a plot expressing the percent copper contributed by relict chalcopyrite. In the projected limit of $|\vec{d}| = 0$ there is no Main Stage modification of the pre-Main Stage assemblage. Although it is very difficult to find samples free of Main Stage effects, the graphical projection through the

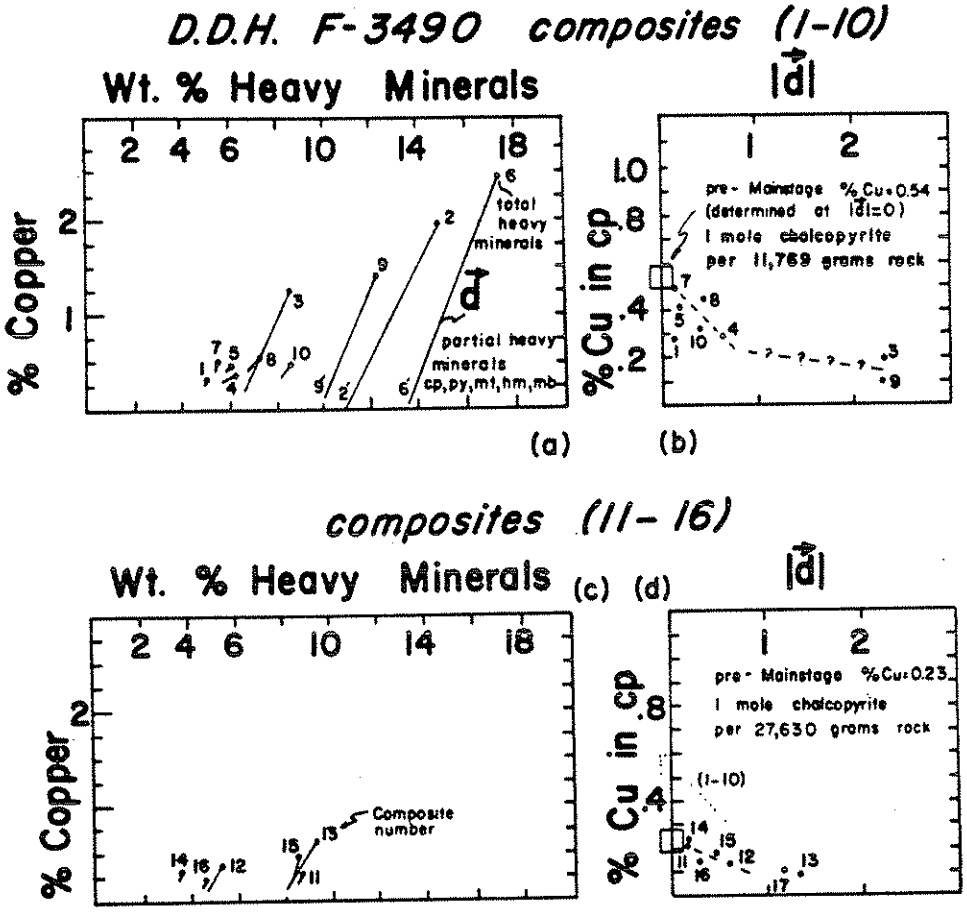

FIG. 4. Gravimetric data for D.D.H. F-3490 subdivided into two groups on the basis of projected initial pre-Main Stage copper grade. Figure 4a depicts the total copper content of each composite (1–10), e.g., 9, 2, or 6, and corresponding copper contents due only to relict chalcopyrite, e.g., 9′, 2′, or 6′. The distance between corresponding points $|\vec{d}|$ is used as a projection parameter in Figure 4b. In the limiting case when $|\vec{d}| = 0$, there is no difference between whole-rock copper content and chalcopyrite contribution, and the percent copper in chalcopyrite represents the initial grade of the rock before Main Stage activity started to destroy chalcopyrite. All pyrite is assigned to the characteristic pre-Main Stage assemblage: chalcopyrite, pyrite, magnetite, hematite (after magnetite), molybdenite. Composites 1 to 10 (Fig. 4b) visually project to an initial copper grade of 0.54 at $|\vec{d}| = 0$. Error of projection is probably about ±0.1 percent Cu. Good positive correlation exists between the parameter $|\vec{d}|$, Main Stage vein density and alteration index I. In Figure 4b, samples 2 and 6 are not plotted as their d value is greater than 3.0. Composites 11 to 16 project to a lower initial copper grade of 0.23 percent Cu (Fig. 4d). All samples are numbered consecutively from the start to the finish of each drill hole.

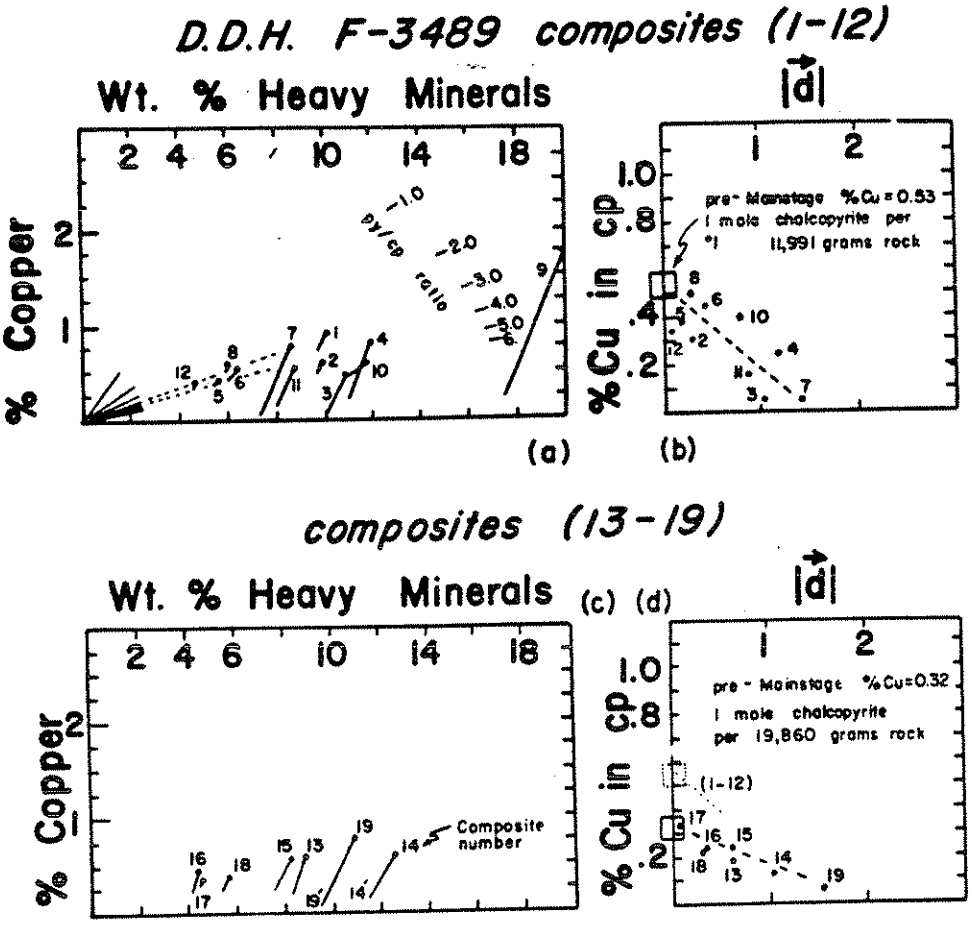

FIG. 5. Gravimetric data for D.D.H. F-3489 composites 1 to 12 (Fig. 5 a, b) and composites 13 to 19 (Fig. 5 c, d). Volumetric pyrite/chalcopyrite ratios are shown in Figure 5a implying an initial ratio of 3 to 4. Notice the difference in initial pre-Main Stage copper grade between composites 1 to 12 and 13 to 19 (Fig. 5d). In Figure 5b, sample 9 is not plotted as its value is greater than 3.0.

data for a suite of altered samples yields unambiguous estimates of initial pre-Main Stage copper grade.

There are basically two potential problems with the method as outlined. Both have been successfully overcome through consideration of a combination of field data and analysis of possible graphical topologies in Figure 3 (a–d). The possibility exists of minor Main Stage chalcopyrite entering into the determination of pre-Main Stage index chalcopyrite, resulting in values of ξ which are too small (equation 13). Furthermore, because of the occurrence of bornite in potassium-silicate assemblages in other porphyry copper deposits, it is possible that in Butte, also, there may be pre-Main Stage bornite, although it is as yet unrecognized. Both of these problems might potentially result in errors in estimation in the original copper content of the pre-Main Stage assemblage. The existence of Main Stage chalcopyrite would cause an estimate of pre-Main Stage copper content to be erroneously high, and a pre-Main Stage bornite-bearing assemblage would be assigned a copper content which would be too low.

Figure 3 depicts hypothetical topologies representative of possible metasomatic reaction types: (a) net copper additive replacement, (b) copper constant replacement, (c) copper extractive replacement, and (d) Main Stage chalcopyrite formation.

Regardless of the type of metasomatic reaction, it is possible to ascertain the salient mechanisms by analysis of graphical topologies. The existence of pre-Main Stage bornite has not been substantiated in numerous optical studies of polished slabs. In no instances could bornite distribution be ascribed to any fractures besides those of Main Stage age. It is possible, however, that exploration efforts on the western side of the Butte district have so far only found the early pyrite-chalcopyrite fringe zone surrounding an early bornite zone.

After consideration of the possible interaction types, those actually operative have been found through laboratory analyses. The major effect upon chalcopyrite is a destruction, either by leaching or replacement, of the pre-Main Stage chalcopyrite. Figures 4 and 5 show representative plots used to derive initial pre-Main Stage grades. Heterogeneities in the initial copper grade are apparent in both D.D.H. F-3489 and F-3490 as the data arrays for composite samples near the end of each hole (Fig. 4, c,d and Fig. 5, c,d) project to lower pre-Main Stage values than those near the start of each drill hole (Fig. 4, a,b and Fig. 5, a,b). The apparent colinearity of the data arrays for a given drill hole intercept strongly suggests that, for the particular intercept length from which the individual composites were taken, the initial pre-Main Stage copper grade was reasonably constant. Using the method outlined it has been possible to reconstruct the distribution of the initial unmodified pre-Main Stage copper grade in a manner far more accurate than is possible with simple magascopic analysis alone. Although there are large cryptic units showing homogeneous pre-Main Stage copper values discovered with the graphical approach, these units are often very hard to recognize visually because of severe modification and local small-scale variability in the pre-Main Stage assemblage. Fortuitously preserved specimens do occasionally persist through Main Stage overprinting in zones of low vein density, but their rarity precludes their systematic usage. These samples with low values of $\vec{d}$ in the graphs do provide the

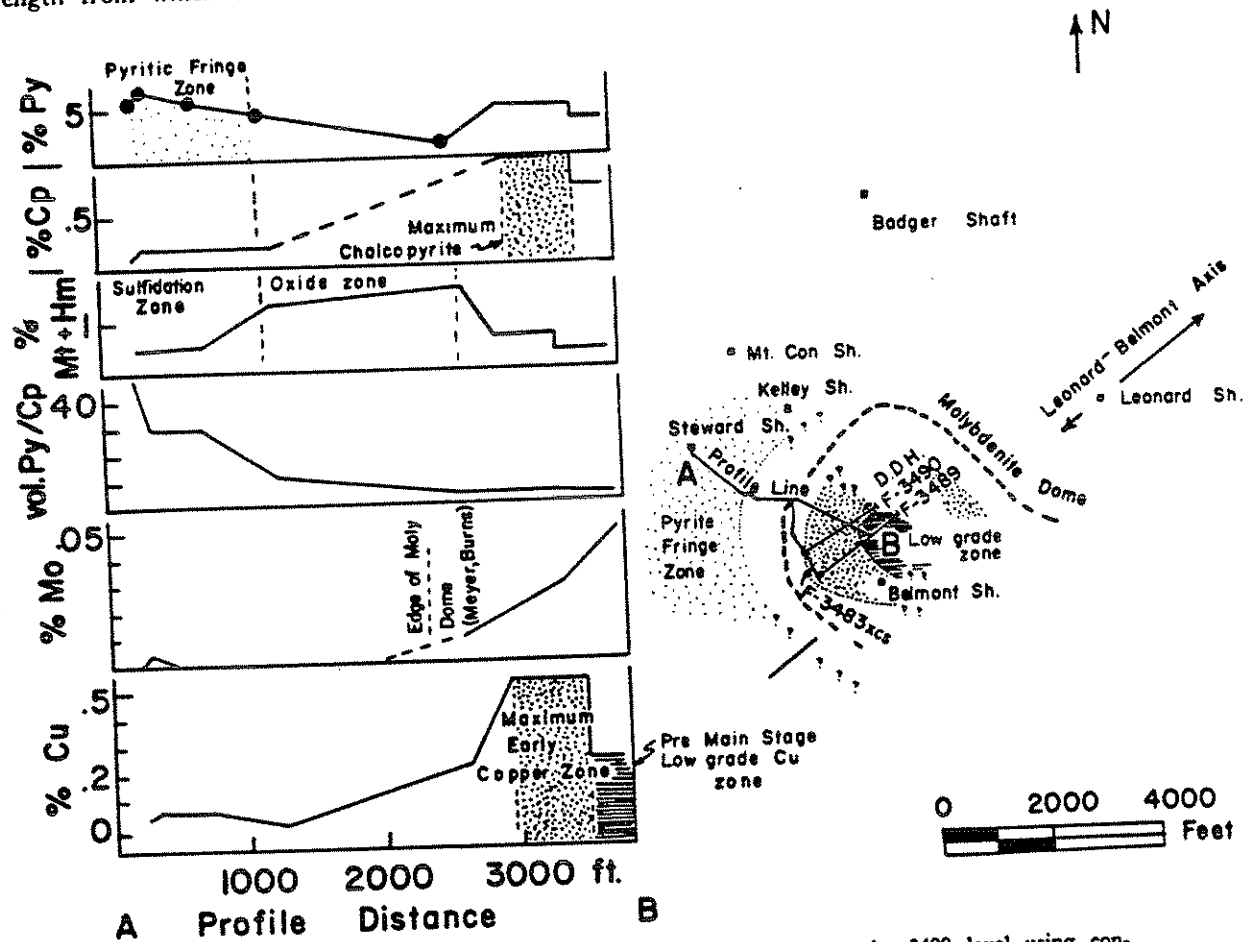

FIG. 6. Distribution of unmodified pre-Main Stage features on the 3400 level using continuous sampling composites from D.D.H. F-3489, F-3490, F-3483 crosscut south (1,491 feet long), and five sampling sites from Steward shaft up to the start of F-3483 XCS, each composed of one fresh-rock sample and one altered sample. Molybdenite dome structure contour on 3400 level is given for reference. Abbreviations used: py (pyrite), cp (chalcopyrite), mt (magnetite), and hm (hematite). Data represented on profile A-B in conjunction with the 3400 level plan map shows the zonation of the pre-Main Stage effects. A peripheral pyritic fringe zone with volumetric py/cp > 30 surrounds an oxide zone of 1 to 2 weight percent magnetite plus hematite, surrounding the highest grade chalcopyrite zone of 0.5 percent copper, encompassing a low-grade core zone with increasing molybdenum content.

most direct evidence for the initial state of Main Stage alteration and strengthen the graphical deductions made using the more frequent, strongly affected samples.

Results of Lithologic Analysis at Butte

A large-scale exploration program was conducted in 1975 and 1976 by the Anaconda Company, focusing on defining the western edge of the multiple stage ore zone. A major crosscut drive was made on the 3400 level from which fan diamond drilling was performed. Deep diamond drilling from the 2000 level along the Leonard-Belmont axis offered penetrations northeast of the zone explored from the crosscut between the Steward and Belmont shafts (Fig. 6). Although a major portion of the district remains to be explored at depth, especially in the central and eastern portions, preliminary results based on the first two-year drilling program offer insight into the multiple-stage ore deposit at Butte.

Pre-Main Stage zonation

Utilization of the graphical projection methods previously outlined has permitted unambiguous determination of the initial pre-Main Stage copper grade zonation by a conceptual removal of Main Stage modification effects corresponding to an idealized state of Main Stage reaction progress equal to zero. Figure 6 shows these results in plan on the 3400 level, incorporating crosscut and diamond drilling data from the 3400 and 2000 levels, from which other minerologic parameters have been determined in the freshest units available. Pre-Main Stage features are shown in profile A-B as functions of profile distance. Several important zonation features shown in plan emerge from the lithologic analysis. From outside the pre-Main Stage molybdenite zone toward the center of the pattern there is (1) a peripheral pyritic zone with approximately 5 weight percent pyrite, (2) an oxide zone consisting of 1 to 2 percent magnetite plus hematite with a low copper grade contributed by early chalcopyrite, (3) a maximum early copper zone with over 0.5 percent copper, surrounding (4) a lower grade interior zone with approximately 0.2 to 0.3 percent copper and increasing molybdenum grades exceeding 0.05 weight percent Mo. Deep drilling penetrations from the 2000 level prove the existence of a maximum early copper zone inside the north flank of the molybdenite dome structure, implying concentrically zoned pre-Main Stage pattern, or at least one which is axially symmetric about a northwest-trending symmetry plane with parallel bands trending northwest to southeast offset 1,000 to 2,000 feet on either side of the symmetry plane.

Molar mineralogical variation with reaction progress

Superimposed upon the initial pre-Main Stage zonation pattern (Fig. 6) are the overall effects of Main Stage hydrothermal circulation. Figure 1 represents the distribution of the major Main Stage veins and offers an indication of the structural complexity of the multiple stage ore mass, especially its vein-controlled character. The net effects of hydrothermal mineralization and alteration of the initially zoned pre-Main Stage mass may be determined from the data generated in the lithologic analysis. Necessary to the formulation of the Main Stage reaction path are exact information on the initial character of the pre-Main Stage mass, assemblages representing a number of intermediate stages of Main Stage modification, and assemblages representing the penultimate stages of Main Stage activity. All of the necessary data are available in the numerous suites of composite samples which have been subjected to laboratory analysis.

Ultimately the entire Main Stage reaction path may be deduced by using basic principles of conservation of mass and irreversible thermodynamics. Equation (9) offers a direct means of determining the stoichiometric reaction coefficients of minerals in the overall net reactions expressing Main Stage mineralization and alteration of a pre-Main Stage assemblage. The number of moles of each mineral as functions of the reaction progress variable are shown in Figures 7 and 8 in which equation (13) has been used to determine the reaction progress variable, ξ, related directly to the number of moles of index mineral chalcopyrite. The size of the initial open chemical system is conceptually adjusted such that there is 1.0 moles of chalcopyrite at the start of Main Stage modification. Figures 4 and 5 illustrate the size (mass) of the systems for the various initial pre-Main Stage copper grades yielding 1 mole of chalcopyrite at the onset of the Main Stage event. For example, a graphical determination of the initial pre-Main Stage copper grade in F-3489 composites 1 to 12 (Fig. 5) is 0.53 percent copper; 11,991 grams of such rock are required to contain 1.0 moles of chalcopyrite.

Molar variations shown include all mineral species in the rock masses except very minor phases such as zircon and various carbonates. The volumetric properties of wall-rock types, as determined by mapping, are shown by various symbols. Although there is considerable scatter in the data, general trends are obvious which are indicated by visually estimated regression lines. In certain instances interpretation is necessary which is checked in later sections of this paper. Both high- and low-grade initial pre-Main Stage zones are shown. Notice in some instances

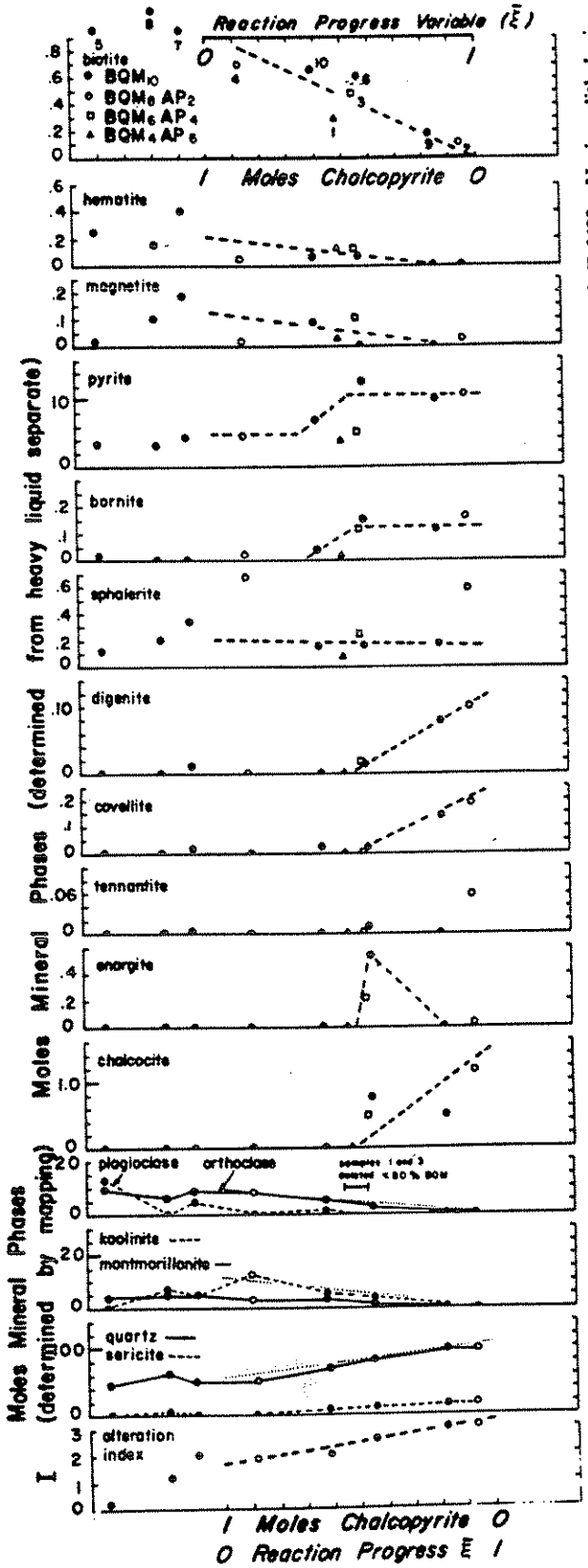

FIG. 7. Molar variation with number of moles chalcopyrite or Main Stage reaction progress variable $\xi = 1 - n$ chalcopyrite for D.D.H. F-3490. Various lithologies are represented by coded symbols (see biotite curve). Biotite, hematite, magnetite, and sphalerite undergo a progressive decrease in molar values with ξ. The inital pre-Main Stage values at $\xi = 0$ are 0.54 percent Cu representing 1 mole of chalcopyrite per 11,769 grams of mineralized rock. Linear visual regressions are shown as dashed lines over various increments of ξ. Composites with significant quantities of rock types other than Butte Quartz Monzonite are given less weight than composites composed entirely of Butte Quartz Monzonite. Notice the simultaneous growth of Main Stage pyrite and bornite, followed by the growth of digenite, covellite, enargite, and chalcocite. Silicate molar variations are determined by alteration mapping. Alteration index is directly proportional to ξ. Notice the alteration index equals 1.5 at $\xi = 0$, implying early Main Stage silicate effects occurred before the chalcopyrite content was modified. Dotted silicate molar variation curves represent conservation of aluminum in the solid phases. Error in molar values is estimated at less than ±10 percent based upon regression of atomic absorption data on heavy mineral separates and calculated metal content, with an average correlation coefficient of 0.94 and standard error of the estimate of 23 percent before a small grain correction of pyrite and chalcopyrite which reduces this error.

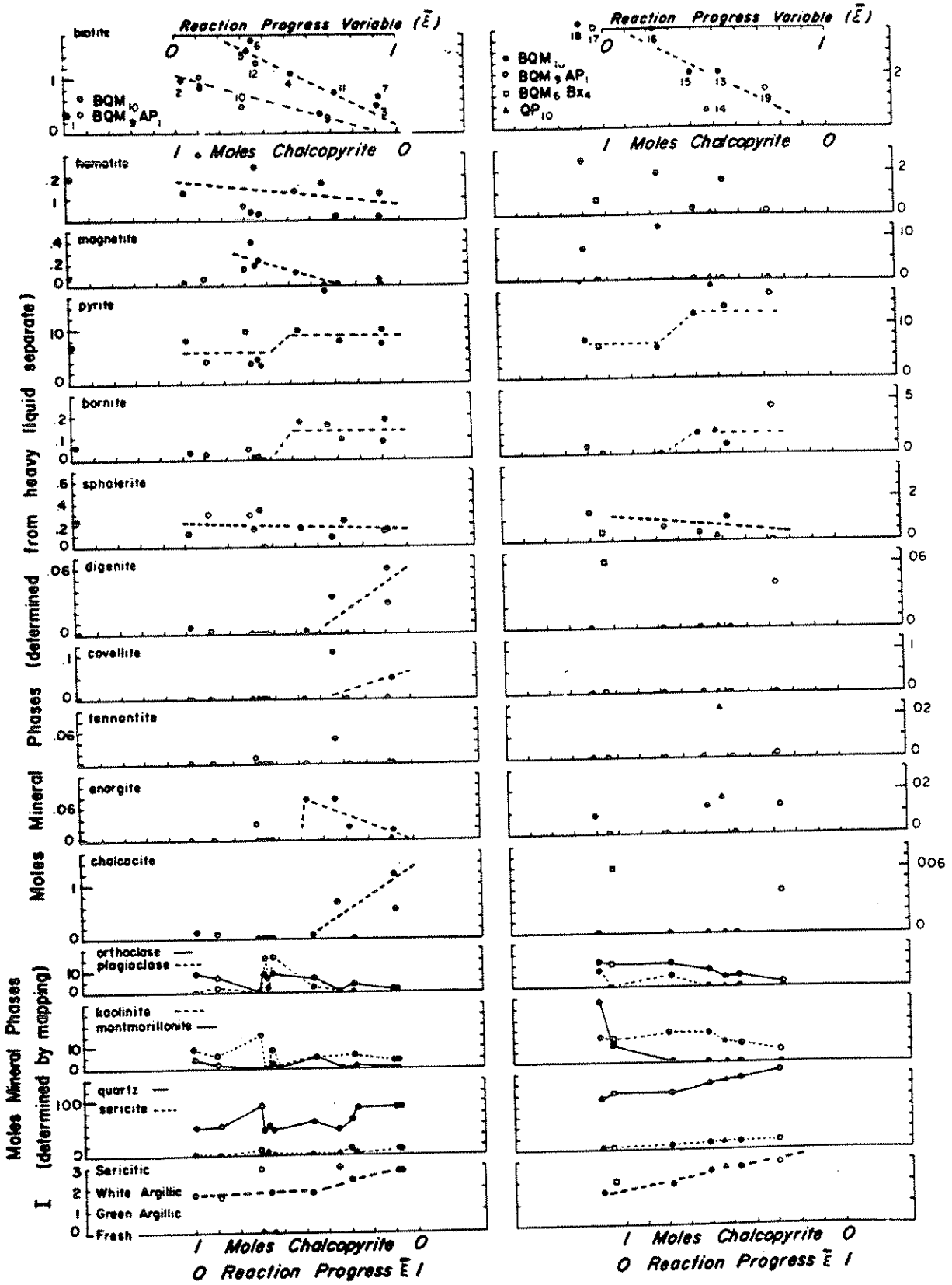
Reaction Progress Variable ($\bar{E}$)
biotite
BQM 10
BQM 9 AP 1
BQM 10
BQM 9 AP 1
BQM 6 Bx 4
QP 10
1 Moles Chalcopyrite 0
hematite
magnetite
pyrite
bornite
sphalerite
digenite
covellite
tennantite
enargite
chalcocite
orthoclase
plagioclase
kaolinite
montmorillonite
quartz
sericite
Sericitic
White Argillic
Green Argillic
Fresh
Moles Mineral Phases (determined from heavy liquid separate)
Moles Mineral Phases (determined by mapping)
0 Reaction Progress $\bar{E}$ 1

that wall rocks with appreciable amounts of lithologic units other than Butte Quartz Monzonite plot off the general trends.

Molar variations with $\bar{\xi}$ are apparent in each of the Figures 7 and 8. Biotite, hematite, magnetite, sphalerite, orthoclase, and kaolinite undergo a more or less monotonic reduction with increasing reaction progress. Plagioclase is converted to montmorillonite which is subsequently converted to kaolinite very early during the reaction as indicated by the alteration index of 1.5 to 2.0 at the start of chalcopyrite modification at $\bar{\xi} = 0$. The choice of chalcopyrite as the index mineral means that the incipient argillic alteration events are not monitored until chalcopyrite destruction begins. At this point the clay products are replaced progressively by sericite. Other possible index minerals exist but, for the present concern of understanding the mass transfer of base metals, chalcopyrite serves a very useful purpose.

Molar values of pyrite remain essentially constant at the pre-Main Stage level up to an intermediate value of $\bar{\xi}$ when there is an unambiguous increase corresponding to an increase in molar bornite. Both of these phases then remain relatively constant during the duration of the Main Stage reaction. Digenite, covellite, enargite, and chalcocite simultaneously appear late in the Main Stage reaction progress sequence. The paragenesis revealed using the reaction progress variable is consistent with the conclusion that pyrite was a stable phase over most of the Main Stage event (Meyer et al., 1968).

Modification of the heavy minerals and silicates in the pre-Main Stage assemblages is accompanied by ever-increasing levels of sericitization and silicification. The ultimate Main Stage effects include complete destruction of feldspars, magnetite, hematite, and biotite with the growth of sericite and quartz as indicated by the dramatic increase of the alteration index, I, with $\bar{\xi}$.

Main Stage reaction stoichiometry

Generalized molar variations with the reaction progress variable, $\bar{\xi}$, are summarized in Figure 9 for D.D.H. F-3490 composites 1–10 representing an average suite of sample material. Linear piecewise continuous functions are shown which seem most reasonable for the data points considered. Nonlinear variation is a possibility but first-order approximations are offered in this study. The apparent linearity may be an indication that the overall reaction is fairly far from attainment of overall equilibrium.

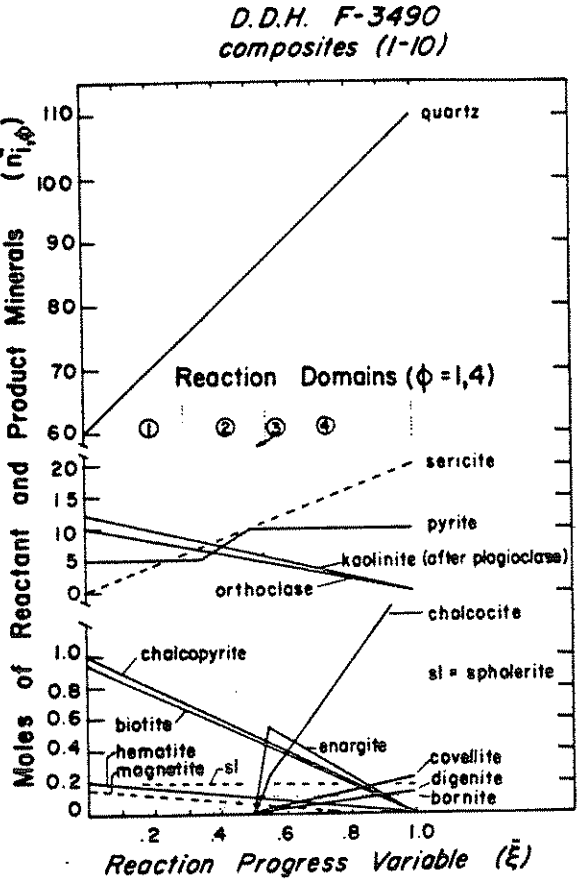

FIG. 9. Generalized molar variation for D.D.H. F-3490 components 1–10. Four reaction domains $\phi = 1, 2, 3$, and 4 are shown defined by the abrupt changes in slope of the piecewise continuous molar curves. Slopes of molar variation curves with reaction progress equal stoichiometric reaction coefficients.

Reaction domains, ϕ, are indicated for various intervals of the reaction progress variable, $\bar{\xi}$, subdivided by abrupt changes in slope of one or more molar curves. Four reaction domains are apparent in most of the material analyzed.

The first reaction domain monitored by chalcopyrite instability, $\phi = 1$, involves a relatively simple growth of sericite and quartz at the expense of all pre-Main Stage minerals except pyrite. The second reaction domain at higher values of $\bar{\xi}$, $\phi = 2$, is characterized by the formation of bornite and a Main Stage growth of pyrite. The third domain results from the simultaneous growth of chalcocite, enargite, covellite, and digenite. The fourth and final reaction domain is characterized by the reduction in enargite content of the Main Stage assemblage.

FIG. 8. Molar variation data for D.D.H. F-3489 depicted for the initial high-grade zone (composites 1–12) and the initial low-grade zone (composites 13–19). Both zones show progressive biotite, magnetite, hematite, and sphalerite destruction. The low-grade portion, however, lacks the systematic development of late-stage chalcocite, covellite, or digenite.

TABLE 1. Main Stage Stoichiometric Equations and Extent of Chemical Reactions for Diamond Drill Hole F-3490 Composites 1 to 10

(11,769 grams of rock with 0.54% Cu pre-Main Stage grade)

		Reaction 1 $0 \leq \xi \leq 0.35$			Reaction 2 $0.35 \leq \xi \leq 0.50$			Reaction 3 $0.50 \leq \xi \leq 0.55$			Reaction 4 $0.55 \leq \xi \leq 1.00$		
	Formula	$n_{i,1}^{0}$	$n_{i,1}^{0.35}$	$\nu_{i,1}$	$n_{i,2}^{0.35}$	$n_{i,2}^{0.50}$	$\nu_{i,2}$	$n_{i,3}^{0.55}$	$n_{i,3}^{0.55}$	$\nu_{i,3}$	$n_{i,4}^{0.55}$	$n_{i,4}^{1.0}$	$\nu_{i,4}$
Reactants													
Chalcopyrite	$CuFeS_2$	1.00	0.65	−1.00	0.65	0.50	−1.00	0.50	0.45	−1.00	0.45	0.0	−1.00
Biotite	$KFe_{2.4}^{+2}Mg_{0.6}^{+2}AlSi_3O_{10}(OH)_2$	0.95	0.62	−0.95	0.62	0.48	−0.95	0.48	0.43	−0.95	0.43	(0.0)	−0.95
Hematite	Fe_2O_3	0.20	0.13	−0.21	0.13	0.10	−0.21	0.10	0.09	−0.21	0.09	(0.0)	−0.21
Magnetite	Fe_3O_4	0.15	0.09	−0.17	0.09	0.06	−0.17	0.06	0.05	−0.17	0.05	(0.0)	−0.17
Sphalerite	ZnS	0.20	0.19	−0.02	0.19	0.19	−0.02	0.19	0.19	−0.02	0.19	0.18	−0.02
Orthoclase	$KAlSi_3O_8$	10.00	6.50	−10.00	6.50	5.00	−10.00	5.00	4.50	−10.00	4.50	0.0	−10.00
Kaolinite	$Al_4Si_4O_{10}(OH)_8$	12.26	7.97	−12.26	7.97	6.13	−12.26	6.13	5.52	−12.26	5.52	0.0	−12.26
Pyrite	FeS_2	5.00	5.00	—	—	—	—	—	—	—	—	—	—
H_2O		—	—	—	—	—	—	•	•	—	—	—	—
Enargite	Cu_3AsS_4	0	0	—	0	0	—	0	0	—	0.55	0.00	−1.22
Cu_{aq}^{+2}		—	—	—	—	—	2.65	•	•	−46.20	•	•	−3.32
K_{aq}^{+}		•	•	−9.05	•	•	−9.05	•	•	−9.05	•	•	−9.05
SO_2		—	—	—	•	•	−67.56	•	•	−49.56	—	—	—
H_{aq}^{+}		••	••	−2.53	—	—	—	—	—	—	—	—	—
Fe_{aq}^{+2}		—	—	—	•	•	−29.85	—	—	—	—	—	—
H_4SiO_{4aq}		•	•	−28.11	•	•	−28.11	•	•	−28.11	•	•	−28.11
$H_3As(OH)_3$		—	—	—	—	—	—	•	•	11.00	—	—	—
O_2		—	—	—	—	—	—	—	—	—	•	•	−2.17
		•	•	−2.85	—	—	—	—	—	—			

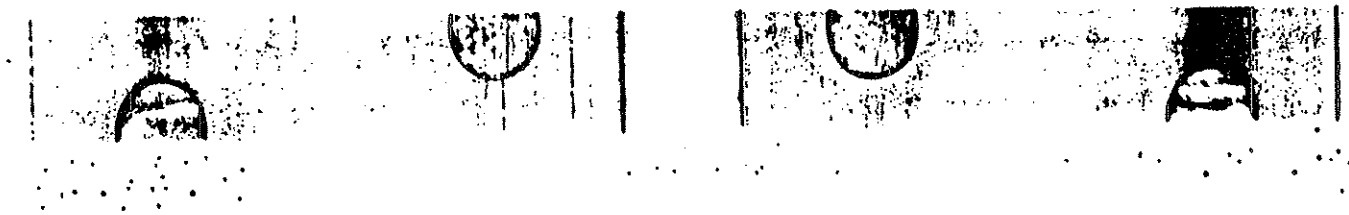

TABLE 1.—(*Continued*)

	Formula	Reaction 1 $0 \le \bar{\xi} \le 0.35$			Reaction 2 $0.35 \le \bar{\xi} \le 0.50$			Reaction 3 $0.50 \le \bar{\xi} \le 0.55$			Reaction 4 $0.55 \le \bar{\xi} \le 1.00$		
		$n_{i,1}^{0}$	$n_{i,1}^{0.35}$	$\nu_{i,1}$	$n_{i,2}^{0.35}$	$n_{i,2}^{0.50}$	$\nu_{i,2}$	$n_{i,3}^{0.50}$	$n_{i,3}^{0.55}$	$\nu_{i,3}$	$n_{i,4}^{0.55}$	$n_{i,4}^{1.0}$	$\nu_{i,4}$
Products													
Pyrite	FeS_2	—	—	—	5.00	10.00	33.33	10.00	10.00	—	10.00	10.00	—
Bornite	Cu_5FeS_4	—	—	—	0.00	0.11	0.73	0.11	0.11	—	0.11	0.11	—
Sericite	$KAl_2Si_3O_{10}(OH)_2$	0.00	7.00	20.00	7.00	10.00	20.00	10.00	11.00	20.00	11.00	20.00	20.00
Quartz	SiO_2	60.00	77.50	50.00	77.5	85.00	50.00	85.00	87.50	50.00	87.50	110.00	50.00
Chalcocite	Cu_2S	0	0	—	0	0	—	0	0.25	5.00	0.25	1.50	2.78
Digenite	Cu_9S_5	0	0	—	0	0	—	0	0.02	0.40	0.02	0.12	0.22
Covellite	CuS	0	0	—	0	0	—	0	0.03	0.60	0.03	0.23	0.44
Enargite	Cu_3AsS_4	0	0	—	0	0	—	0	0.55	11.00	—	—	—
Cu_{aq}^{+2}		•	•	1.00	•	•	—	—	—	—	—	—	—
Fe_{aq}^{+2}		•	•	4.21	—	—	—	•	•	4.21	•	•	4.21
SO_4		•	•	2.02	—	—	—	—	—	—	•	•	2.58
Mg_{aq}^{+2}		•	•	0.57	•	•	0.57	•	•	0.57	•	•	0.57
Zn_{aq}^{+2}		•	•	0.02	•	•	0.02	•	•	0.02	•	•	0.02
H_2O		•	•	87.48	•	•	49.78	—	—	78.79	•	•	78.90
H^+		—	—	—	••	••	72.87	••	••	91.85	••	••	6.09
O_2		—	—	—	•	•	85.59	•	•	80.58	—	—	—
$H_3As(OH)_3$		—	—	—	—	—	—	—	—	—	•	•	1.22

Note: (—) Species does not participate on this side of reaction. (*) Stoichiometric coefficients determined by conservation of mass. (**) Stoichiometric coefficients determined by conservation of charge.

Aluminum conservation in solid species has been maintained. Biotite composition is an average of probe data on material within the molybdenite dome (Roberts, 1973; Brimhall, 1973).

TABLE 2. Main Stage Stoichiometric Equations and Extent of Chemical Reactions for Diamond Drill Hole F-3489 Composites 1 to 12

(11,991 grams of rock with 0.53% Cu pre-Main Stage grade)

		Reaction 1 $0 \leq \xi \leq 0.40$			Reaction 2 $0.40 \leq \xi \leq 0.50$			Reaction 3 $0.50 \leq \xi \leq 0.53$			Reaction 4 $0.53 \leq \xi \leq 1.00$		
	Formula	$n_{i,1}^{0}$	$n_{i,1}^{0.40}$	$\nu_{i,1}$	$n_{i,2}^{0.40}$	$n_{i,2}^{0.50}$	$\nu_{i,2}$	$n_{i,3}^{0.50}$	$n_{i,3}^{0.53}$	$\nu_{i,3}$	$n_{i,4}^{0.53}$	$n_{i,4}^{1.0}$	$\nu_{i,4}$
Reactants													
Chalcopyrite	$CuFeS_2$	1.00	0.60	−1.00	0.60	0.50	−1.00	0.50	0.47	−1.00	0.47	0.0	−1.00
Biotite	$KFe_{2.4}^{+2}Mg_{0.6}^{+2}AlSi_3O_{10}(OH)_2$	(1.10)	0.66	−1.10	0.66	0.55	−1.10	0.55	0.52	−1.10	0.52	0.0	−1.10
Hematite	Fe_2O_3	0.18	0.13	−0.13	0.13	0.12	−0.13	0.12	0.12	−0.13	0.12	0.06	−0.13
Magnetite	Fe_3O_4	0.46	0.29	−0.42	0.29	0.25	−0.42	0.25	0.24	−0.42	0.24	(0.0)	−0.42
Sphalerite	ZnS	0.25	0.22	−0.07	0.22	0.21	−0.07	0.21	0.21	−0.07	0.21	0.18	−0.07
Orthoclase	$KAlSi_3O_8$	9.00	5.40	−9.00	5.40	4.50	−9.00	4.50	4.20	−9.00	4.20	0.0	−9.00
Kaolinite	$Al_4Si_4O_{10}(OH)_8$	9.48	5.69	−9.48	5.69	4.74	−9.48	4.74	4.46	−9.48	4.46	0.0	−9.48
Pyrite	FeS_2	6.00	6.00	—	—	—	—	—	—	—	—	—	—
H_2O		—	—	—	•	•	—	•	•	—	—	—	—
Enargite	Cu_3AsS_4	0	0	—	0	0	—	0	0	—	0.08	0.0	−0.17
Cu_{aq}^{+2}		—	—	—	•	•	−6.50	•	•	−7.01	•	•	−5.33
K_{aq}^{+}		•	•	−5.90	•	•	−5.90	•	•	−5.90	•	•	−5.90
SO_2		—	—	—	—	—	−57.93	•	•	−8.61	•	•	−0.80
H_{aq}^{+}		••	••	−7.88	—	—	—	—	—	—	—	—	—
Fe_{aq}^{+2}		—	—	—	•	•	−23.34	—	—	—	—	—	—
H_4SiO_{4aq}		•	•	−14.78	•	•	−14.78	—	—	−14.78	•	•	−14.78
$H_3As(OH)_3$		—	—	—	—	—	—	•	•	−2.67	—	—	—
O_2		•	•	−2.82	•	•	—	—	—	—	•	•	—

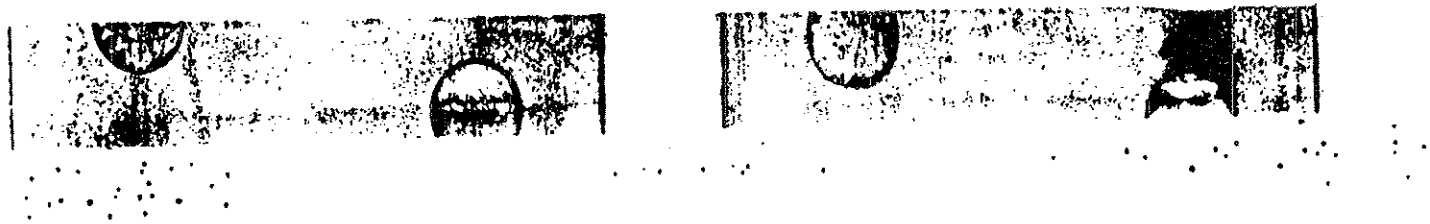

TABLE 2—(*Continued*)

	Formula	Reaction 1 $0 \le \xi \le 0.40$			Reaction 2 $0.40 \le \xi \le 0.50$			Reaction 3 $0.50 \le \xi \le 0.53$			Reaction 4 $0.53 \le \xi \le 1.00$		
		$n_{i,1}^{0}$	$n_{i,1}^{0.40}$	$\nu_{i,1}$	$n_{i,2}^{0.40}$	$n_{i,2}^{0.50}$	$\nu_{i,2}$	$n_{i,3}^{0.50}$	$n_{i,3}^{0.53}$	$\nu_{i,3}$	$n_{i,4}^{0.53}$	$n_{i,4}^{1.0}$	$\nu_{i,4}$
Products													
Pyrite	FeS_2	—	—	—	6.00	8.70	27.00	8.70	8.70	—	8.70	8.70	—
Bornite	Cu_5FeS_4	—	—	—	0.00	0.15	1.50	0.15	0.15	—	0.15	0.15	—
Sericite	$KAl_3Si_3O_{10}(OH)_2$	0.0	6.40	16.00	6.40	8.00	16.00	8.00	8.48	16.00	8.48	16.00	16.00
Quartz	SiO_2	45.00	59.00	35.00	59.00	62.50	35.00	62.50	63.60	35.00	63.80	80.00	35.00
Chalcocite	Cu_2S	0	0	—	0	0	—	0	0	—	0	1.30	2.77
Digenite	Cu_9S_5	0	0	—	0	0	—	0	0	—	0	0.06	0.13
Covellite	CuS	0	0	—	0	0	—	0	0	—	0	0.06	0.13
Enargite	Cu_3AsS_4	0	0	—	0	0	—	0.0	0.08	2.67	—	—	—
Cu_{aq}^{+2}		•	•	1.00	—	—	—	—	—	—	—	—	—
Fe_{aq}^{+2}		•	•	5.16	—	—	—	•	•	5.16	•	•	5.16
SO_4		•	•	2.07	•	•	—	—	—	—	—	—	—
Mg_{aq}^{+2}		•	•	0.66	•	•	0.66	•	•	0.66	•	•	0.66
Zn_{aq}^{+2}		•	•	0.07	•	•	0.07	•	•	0.07	•	•	0.07
H_2O		•	•	56.52	—	—	20.52	—	—	57.86	•	•	49.60
H^+		—	—	—	••	••	64.12	••	••	8.14	••	••	4.78
O_2		—	—	—	—	—	75.19	•	•	13.87	—	—	3.09
$H_3As(OH)_6$		—	—	—	—	—	—	—	—	—	•	•	0.17

Note: (—) Species does not participate on this side of reaction. (•) Stoichiometric coefficients determined by conservation of mass. (••) Stoichiometric coefficients determined by conservation of charge.

Aluminum conservation in solid species has been maintained.

TABLE 3. Main Stage Stoichiometric Equations for Diamond Drill Hole F-3490 Composites 1 to 10 (11,769 grams of rock with 0.54% pre-Main Stage copper grade)

Reactants	Products
$0 \leq \bar{\xi} \leq 0.35$	
1.00 chalcopyrite + 0.95 biotite + 0.21 hematite + 0.17 magnetite + 0.02 sphalerite + 10.0 orthoclase + 12.26 kaolinite + 9.05 K^+ + 2.53 H^+ + 28.11 H_4SiO_4 + 2.85 O_2	20.0 sericite + 50.0 quartz + 1.0 Cu^{+2} + 4.20 Fe^{+2} + 2.02 SO_2 + 0.57 Mg^{+2} + 0.02 Zn^{+2} + 87.48 H_2O
$0.35 \leq \bar{\xi} \leq 0.50$	
1.00 chalcopyrite + 0.95 biotite + 0.21 hematite + 0.17 magnetite + 0.02 <sphalerite + 10.0 orthoclase + 12.26 kaolinite + 9.05 K^+ + 67.56 SO_2 + 29.85 Fe^{+2} + 28.11 H_4SiO_4 + 2.65 Cu^{+2}	33.33 pyrite + 0.73 bornite + 20.0 sericite + 50.0 quartz + 0.57 Mg^{+2} + 0.02 Zn^{+2} + 49.78 H_2O + 72.87 H^+ + 85.59 O_2
$0.50 \leq \bar{\xi} \leq 0.55$	
1.00 chalcopyrite + 0.95 biotite + 0.21 hematite + 0.17 magnetite + 0.02 sphalerite + 10.0 orthoclase + 12.26 kaolinite + 46.20 Cu^{+2} + 9.05 K^+ + 49.56 SO_2 + 28.11 H_4SiO_4 + 11.0 $H_3As(OH)_3$	20.00 sericite + 50.0 quartz + 5.0 chalcocite + 0.40 digenite + 0.60 covellite + 11.00 enargite + 4.21 Fe^{+2} + 0.57 Mg^{+2} + 0.02 Zn^{+2} + 91.85 H^+ + 80.58 O_2 + 78.79 H_2O
$0.55 \leq \bar{\xi} \leq 1.00$	
1.00 chalcopyrite + 0.95 biotite + 0.21 hematite + 0.17 magnetite + 0.02 sphalerite + 10 orthoclase + 12.26 kaolinite + 1.22 enargite + 3.32 Cu^{+2} + 9.05 K^+ + 28.11 H_4SiO_4 + 2.17 O_2	20.0 sericite + 50.0 quartz + 2.78 chalcocite + 0.22 digenite + 0.44 covellite + 4.21 Fe^{+2} + 2.58 SO_2 + 0.57 Mg^{+2} + 0.02 Zn^{+2} + 78.90 H_2O + 6.09 H^+ + 1.22 $H_3As(OH)_3$

Over each reaction interval, equation (9) may be used to calculate the stoichiometric reaction coefficients of the minerals taking part in the overall chemical reaction. Tables 1 and 2 present the mineralogical data necessary to calculate the reaction progress variable, $\bar{\xi}$, including the number of moles of each mineral at the start and end of each reaction interval. The complete heterogeneous chemical reactions representing mass transfer by internal and external processes are given utilizing charge balance of aqueous species and conservation of mass in the overall reaction, but not necessarily in the solid species. Each reaction is written with the stoichiometric coefficient of the index species, chalcopyrite, equal to one, with an initial molar value of 1.0 for chalcopyrite. Visually estimated regression lines of the silicate species produce a near-aluminum balance among the solid reactants and product species. The regression lines have consequently been slightly adjusted to give an exact conservation of aluminum in the solids.

TABLE 4. Main Stage Stoichiometric Equations for Diamond Drill Hole F-3489 Composites 1–12 (11,991 grams of rock with 0.53% pre-Main Stage copper grade).

Reactants	Products
$0 \leq \bar{\xi} \leq 0.40$	
1.00 chalcopyrite + 1.10 biotite + 0.13 hematite + 0.42 magnetite + 0.07 sphalerite + 9.00 orthoclase + 9.48 kaolinite + 5.90 K^+ + 7.88 H^+ + 14.78 H_4SiO_4 + 2.82 O_2	16.00 sericite + 35.00 quartz + 1.00 Cu^{+2} + 5.16 Fe^{+2} + 2.07 SO_2 + 0.66 Mg^{+2} + 0.07 Zn^{+2} + 56.52 H_2O
$0.40 \leq \bar{\xi} \leq 0.50$	
1.00 chalcopyrite + 1.10 biotite + 0.13 hematite + 0.42 magnetite + 0.07 sphalerite + 9.00 orthoclase + 9.48 kaolinite + 6.50 Cu^{+2} + 5.90 K + 23.34 Fe^{+2} + 14.78 H_4SiO_4 + 57.93 SO_2	27.00 pyrite + 1.50 bornite + 16.00 sericite + 35.00 quartz + 0.66 Mg^{+2} + 0.07 Zn^{+2} + 64.12 H^+ + 75.19 O_2 + 20.52 H_2O
$0.50 \leq \bar{\xi} \leq 0.53$	
1.00 chalcopyrite + 1.10 biotite + 0.13 hematite + 0.42 magnetite + 0.07 sphalerite + 9.00 orthoclase + 9.48 kaolinite + 7.01 Cu^{+2} + 5.90 K^+ + 8.61 SO_2 + 14.78 H_4SiO_4 + 2.67 $H_3As(OH)_3$	16.00 sericite + quartz + 2.67 enargite + 5.16 Fe^{+2} + 0.66 Mg^{+2} + 0.07 Zn^{+2} + 8.14 H^+ + 13.87 O_2 + 57.86 H_2O
$0.53 \leq \bar{\xi}$ 1.00	
1.00 chalcopyrite + 1.10 biotite + 0.13 hematite + 0.42 magnetite + 0.07 sphalerite + 9.00 orthoclase + 9.48 kaolinite + 0.17 enargite + 5.33 Cu^{+2} + 5.90 K^+ + 0.80 SO_2 + 14.78 H_4SiO_4	16.00 sericite + 35.00 quartz + 2.77 chalcocite + 0.13 digenite + 0.13 covellite + 5.16 Fe^{+2} + 0.66 Mg^{+2} + 0.07 Zn^{+2} + 49.60 H_2O + 4.78 H^+ + 0.17 $H_3As(OH)_3$ + 3.09 O_2

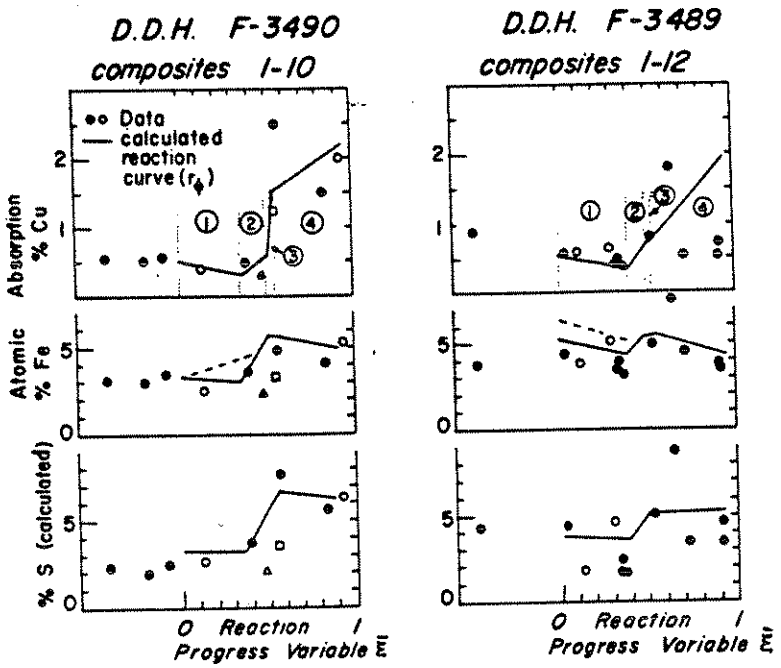

FIG. 10. Comparison of composite Cu, Fe, S assay data with calculated total element content curves for the net chemical reactions derived from molar variation with $\bar{\xi}$ plots. Reaction domains $\phi = 1, 2, 3$, and 4 are shown.

The net Main Stage stoichiometric equations are given in Tables 3 and 4 for each reaction interval of $\bar{\xi}$. Comparison of the equations for the two drill holes reveals a general similarity in the position of the aqueous species appearing as reactants or products. Considering the reactions as interchanges between rock and aqueous fluid, the aqueous species represent the vehicle for the physical transfer of mass in or out of the system via the hydrothermal fluid. It is possible, then, to consider the position of the aqueous species as a source or sink of mobile constituents moving freely between the mineralized rock and reactive fluid.

In reaction interval 1, $0 \leq \bar{\xi} \leq 0.35$ for D.D.H. F-3490 and $0 \leq \bar{\xi} \leq 0.40$ for D.D.H. F-3489; copper, iron, magnesium, zinc, and sulfur are removed from the rock by the aqueous fluids which contribute potassium and aqueous silica to the rock.

In the relatively short reaction interval 2, $0.35 \leq \bar{\xi} \leq 0.50$ for D.D.H. F-3490 and $0.40 \leq \bar{\xi} \leq 0.50$ for D.D.H. F-3489; copper, iron, and sulfur are removed from the fluid during the precipitation interval of pyrite and bornite.

Reaction interval 3 involves a slight variation between the two diamond drill holes shown. Although copper, sulfur, and arsenic are extracted from the fluid in both instances over an interval of $0.50 \leq \bar{\xi} \leq 0.55$ for D.D.H. F-3490 and $0.50 \leq \bar{\xi} \leq 0.53$ for D.D.H. F-3489, chalcocite, digenite, and covellite form in the former drill hole in addition to the enargite precipitated in both instances.

Reaction interval 4 is very similar for both diamond drill holes. $0.55 \leq \bar{\xi} \leq 1.0$ for D.D.H. F-3490 and $0.53 \leq \bar{\xi} \leq 1.0$ for D.D.H. F-3489. Enargite is consumed with continued copper fixation in the rock accompanied by iron liberation into the fluid.

In Figure 10, elemental variation with reaction progress variable, $\bar{\xi}$, as determined by atomic absorption analysis of whole-rock composites, is compared with calculated reaction curves for each of the four reaction intervals. $\phi = 1$ to 4, determined by estimated regression of molar mineral data, charge balance, and conservation of mass within the overall reaction. Mass tranfser between the fluid and rock is obvious as there is substantial variation in element content with $\bar{\xi}$ implying addition for increasing element functions and extraction for decreasing functions with reaction progress. Although the calculated curves are not determined independently of the measured data points, the general agreement implies an internal consistency to the stoichiometric equations. Furthermore, the calculated reaction curves serve a useful interpretive purpose when molar variation with $\bar{\xi}$ is somewhat ambiguous. The calculated iron curve for D.D.H. F-3490 is depicted in two manners. Over reaction interval one, a dashed line is shown which represents pyrite formation from the onset of Main

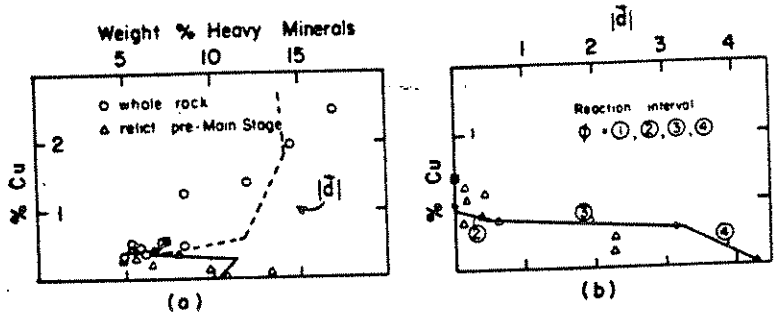

FIG. 11. Comparison of graphical projection method with calculated reaction curves. Figure 11a depicts the percent Cu and weight percent heavy minerals and Figure 11b shows the projection to $|\bar{d}| = 0$ at the onset of the Main Stage event. In both cases, the calculated curves are piecewise continuous functions. D.D.H. F-3490 is shown. Reaction domains $\phi = 1, 2, 3$, and 4 are depicted in Figure 11b.

Stage at $\bar{\xi} = 0$. A solid line is also shown for the same reaction interval for no pyrite formation until interval 2, which is a much better fit to the data points determined by atomic absorption methods. Similarly for D.D.H. F-3489 a dashed line is shown representing biotite content which is erroneously high due to gangue mineral contamination.

Verification of the analytic method

The basic assumption in the lithologic method is that the initial pre-Main Stage copper grade can be accurately determined. The method used involves a graphical projection of data points representing various intermediate states of Main Stage modification of the early ore mass. Using the stoichiometric equations it is possible to calculate the interpreted behavior of the assemblages in the same coordinate system used initially to find the pre-Main Stage grade. Figure 11 shows the raw gravimetric data used to determine the initial copper grade of D.D.H. F-3490 including whole-rock values and relict chalcopyrite data. In addition, calculated curves are shown derived from the stoichiometric equations which have been determined from molar variation with $\bar{\xi}$ plots. Several features are important, especially the piecewise continuous nature of the calculated graphs. Use of the graphical projection using visual inspection in a limiting case of $|\bar{d}| = 0$ corresponding to $\bar{\xi} = 0$ is reasonable as long as a good number of samples are used spanning a significant interval of Main Stage effects including at least a few samples which are relatively unaltered. Otherwise estimates of the initial copper grade may be too low as evidenced by the vertical slope of reaction interval one in Figure 11b.

After analyzing the potential problems associated with the graphical projection method yielding an idealized initial state of the pre-Main Stage effects, the method remains as a useful and accurate technique. In zones where late-stage hydrothermal effects are very intense and collection of a suite of large samples representing a range of alteration levels is unfeasible, the determination of the initial state of the system requires special care. In this instance, it may become necessary to use sampling intervals which are relatively small, e.g., less than 10 feet long and to define composite samples in such a way as to use the freshest units available.

Discussion

By using the rock-analysis methods outlined in this paper, one can deduce the original early hydrothermal zonation in the western edge of the zone of multiple stage mineralization without the Main Stage modification effects of the pre-Main Stage ore mass. Pre-Main Stage zoning patterns seem most closely linked to east-west-trending Steward-type quartz porphyry dikes which parallel in detail major early hydrothermal features and introduce the first important disseminated copper in the form of marginal biotitic breccias.

Main Stage vein systems, superimposed upon the early alteration and mineralization pattern, may be related to hydrothermal circulation driven by a heat source younger than the Steward-type parent magma, offset somewhat northward in the area of the Modoc intrusive system in the Leonard mine.

Several conclusions may be drawn concerning the origin of Main Stage vein material which are based upon the nature of the fluid-rock interaction mechanisms.

The hypogene process of element recycling: leaching and enrichment

The overall hydrothermal processes operative during the Main Stage modification of the early mineralized mass may be unambiguously derived from consideration of mass-transfer relations in open chemical systems determined by quantitative lithological analysis. Figure 12 presents a summary of the

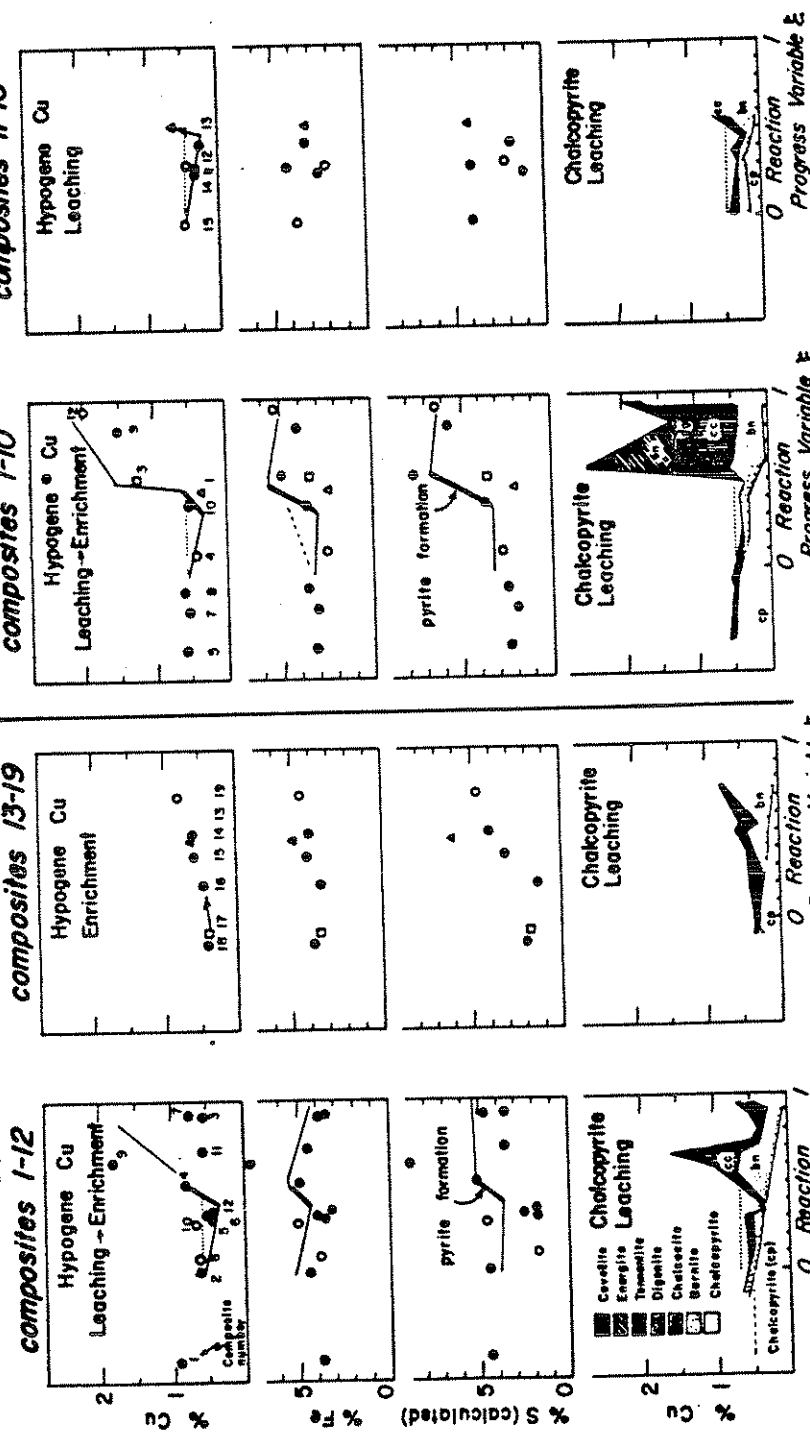

FIG. 12. Diamond drilling data for two parallel holes, F-3489 and F-3490, as a function of Main Stage reaction progress variable, ξ, where $\xi = 1$ —moles of chalcopyrite determined gravimetrically. Both drill holes have been divided into two initial pre-Main Stage grade zones: D.D.H. F-3489 composites 1 to 12 and 13 to 19 and D.D.H. F-3490 composites 1 to 10 and 11 to 16. Composite numbers are given consecutively along each drill hole. Figure 12a, b, and c show, respectively, the variation of percent copper, iron, and sulfur with reaction progress variable, ξ. Copper and iron are atomic absorption data, sulfur is calculated. Figure 12d depicts the mineralogical effects producing the observed variation in total copper content with reaction progress variable, ξ. In all cases note the initial hypogene chalcopyrite leaching with relatively late formation of bornite followed by chalcocite, digenite, tennantite, enargite, and covellite.

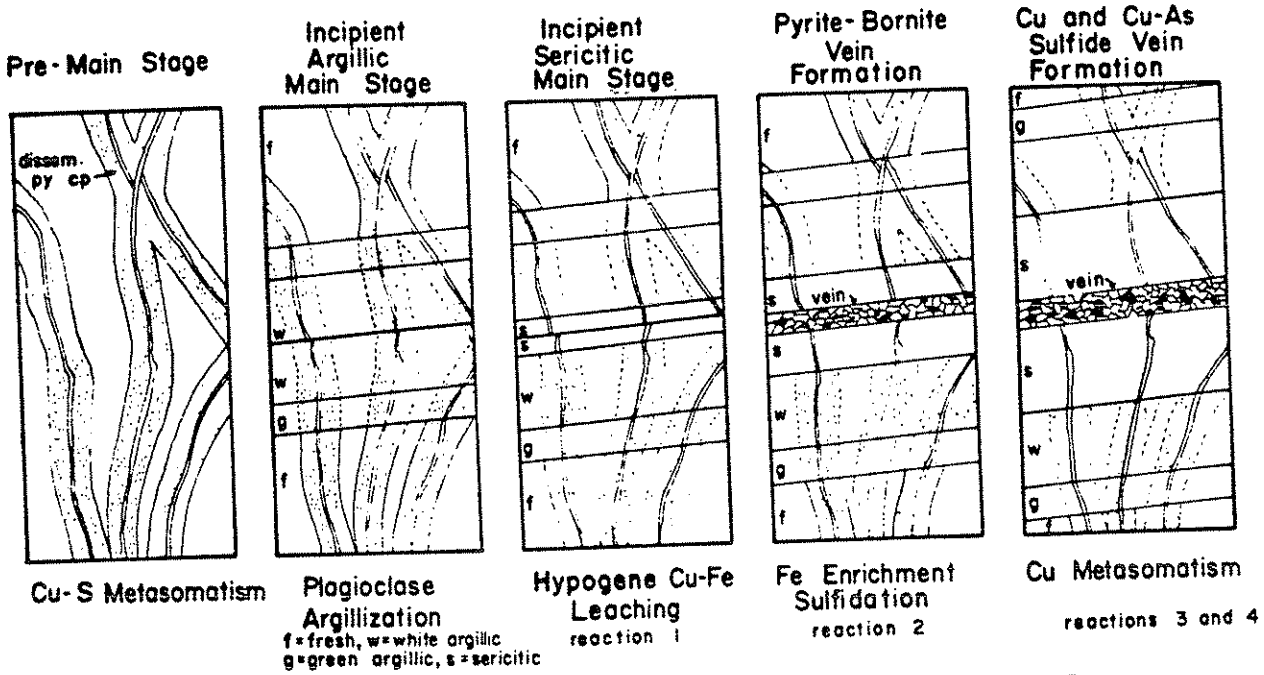

FIG. 13. Summary of idealized Main Stage vein-forming events. Initial pre-Main Stage mineralization is within the alteration halos of K-silicate assemblages. Main Stage hydrothermal effects proceed outward from fractures with progressive superposition of more intense alteration effects upon the early, fracture-controlled disseminated mineralization. Simultaneous hypogene leaching of disseminated chalcopyrite and copper fixation in veins is shown.

element and mineralogical variation with Main Stage reaction progress for drill hole penetrations into the high-grade portion as well as the low-grade core zone of the early ore mass on the western side of the Butte district. Following an incipient argillic alteration phase, hypogene chalcopyrite leaching results in a relatively prolonged initial interval of copper, iron, and sulfur extraction from the mineralized wall rock by the hydrothermal fluids.

At intermediate values of reaction progress, $\bar{\xi} > 0.5$, the formation of Main Stage pyrite and other sulfides produce an overall copper addition or hypogene enrichment in the form of high-grade vein structures surrounded in detail by a leached halo of sericitized wall rock depleted in its early chalcopyrite content (Fig. 13). Molybdenite, in contrast, appears to be relatively inert during intense sericitization.

The initial pre-Main Stage copper grade appears to influence the mineralogical nature of subsequent reactions. In Figure 12 two diamond drill holes are shown with two composite groups for each drill hole. In both cases composites with low numbers represent the high-grade zone of the pre-Main Stage pattern and high-number composites represent the low-grade core zone. Reactions in the high-grade mass produce an initial leaching interval followed by pyrite-bornite formation without chalcocite, digenite, enargite, or covellite until the very late stages of reaction progress. In contrast, reactions in the low-grade core zone produce bornite and some chalcocite eventually, but digenite, enargite, and covellite are completely lacking even at high values of reaction progress. It is possible that the Main Stage reactions proceeding in the low-grade core zone represent somewhat juvenile stages in the development of intense Main Stage mineralization.

The progressive leaching of pre-Main Stage chalcopyrite, from both low- and high-grade zones, results initially in a whole-rock copper and iron depletion. This reaction interval obviously represents a potential source of Main Stage vein-forming constituents. In the area studied in this paper, initial copper depletion by Main Stage fluids has generally been followed by copper addition producing a multiple stage ore mass with a copper grade actually enhanced by the net effects of late-stage modification. However, on a districtwide scale, a possibility exists that there are net depletion zones in the pre-Main Stage pattern as proposed in the genetic model of the Creede Mining district (Barton et al., 1977) and observed on a small scale in central Peru (Lacy and Hosmer, 1956).

Interpretation of the Solution Chemistry

Construction of isothermal activity diagrams showing log $a_{Fe^{+2}}/a_{H^+}^2$ as a function of log a_{Cu^+}/a_{H^+} at

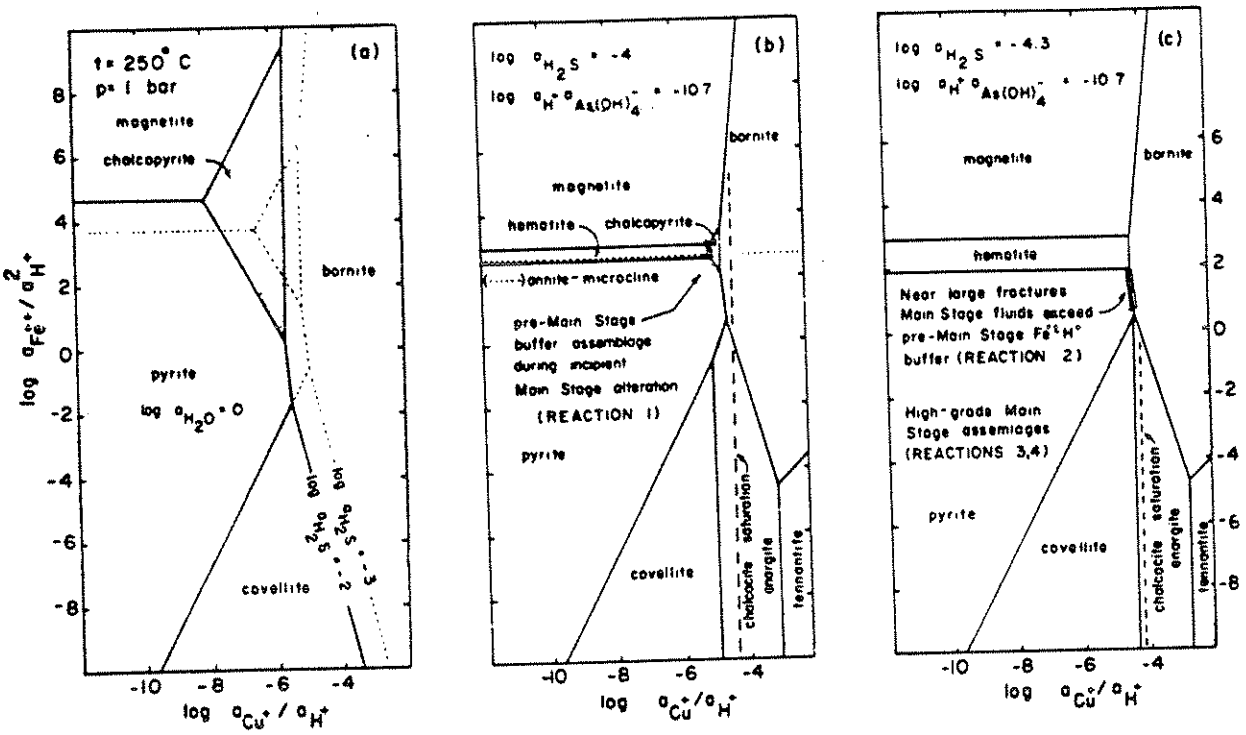

FIG. 14. Theoretical activity diagrams at 250°C and 1 bar, representing the phase stability of magnetite, hematite, pyrite, covellite, bornite, chalcopyrite, and enargite. Figure 14a depicts an arsenic-free system at $a_{H_2O} = 1.0$ for a log $a_{H_2S} = -2.0$ (solid) and log $a_{H_2S} = -3$ (dashed) showing the shrinkage of the chalcopyrite field at lower H_2S activities. Notice that there is no hematite field between pyrite and magnetite. Figure 14b shows an arsenic-bearing system with log $(a_{H^+} a_{As(OH)_4^-}) = -10.7$, log $a_{H_2O} = 1.0$, and log $a_{H_2S} = -4$. The chalcopyrite field is very small at the low activity of H_2S, and a hematite field has appeared between the fields of magnetite and pyrite. An idealized silicate buffer assemblage of annite-microcline is shown. The solution composition in equilibrium with the pre-Main Stage assemblage is depicted with a dotted pattern, spanning a very limited compositional range. The chalcocite saturation line is shown, as are the fields of bornite, covellite, enargite, and tennantite. Figure 14c is an isothermal section at a log $(a_{H^+} a_{As(OH)_4^-}) = -10.7$, $a_{H_2O} = 1$, and log $a_{H_2S} = -4.3$ shown to depict possible solution compositions during late Main Stage reactions. The chalcopyrite field has disappeared. Irreversible reactions, $\phi = 1$ and 2, may reduce the log $a_{Fe^{+2}}/a^{2H^+}$ in the absence of a chalcopyrite, until saturation is attained with respect to covellite, enargite, or chalcocite. The log a_{Cu^+}/a_{H^+} remains essentially constant.

250°C provides a convenient framework in which to interpret the Main Stage reaction chemistry in terms of phase equilibria. The equilibrium constants were taken directly from the literature (Helgeson, 1969; Knight, 1977) and are internally consistent, but nevertheless errors may be present which could potentially affect the topology of the calculated activity diagrams (Table 5).

The pre-Main Stage potassium assemblage consists of chalcopyrite, pyrite, biotite, orthoclase, muscovite, anhydrite, quartz, and magnetite. During the early stages of Main Stage alteration magnetite is partially oxidized to hematite and the Butte Quartz Monzonite plagioclase is converted to clays. This behavior may be represented in multidimensional activity space showing log $a_{Fe^{+2}}/a_{H^+}^2$ vs. log a_{Cu^+}/a_{H^+} contoured on constant log a_{H_2S}, log a_{H_2O}, and log $(a_{H^+} a_{As(OH)_4^-})$. As shown in Figure 14a, the chalcopyrite field rapidly shrinks with decreasing log a_{H_2S} or increasing state of oxidation in the fluid phase. As pointed out by Knight (1977), pyrite gives way to magnetite at high iron-activity ratios if the H_2S activity is small (i.e., under reducing conditions). Whenever a hematite stability field appears, its boundary with respect to magnetite is independent of the activity of H_2S or arsenic activity. Under these conditions the chalcopyrite field is very small or absent (if log $a_{H_2S} < -4.2$) (Fig. 14a,b). Consequently, the possible values of log a_{H_2S} are very restricted (approximately −4.0 to −4.2) for the pre-Main Stage chalcopyrite to coexist with one of two assemblages: magnetite-hematite or hematite-pyrite. In addition, the log $a_{Fe^{+2}}/a_{H^+}^2$ is very restricted. As the activity of H_2S diminishes and the chalcopyrite field shrinks (Fig. 14b), the log $a_{Fe^{+2}}/a_{H^+}^2$ is 2.95 for the magnetite-hematite-chal-

copyrite assemblage and 2.52 for the hematite-pyrite-chalcopyrite assemblage at a log $a_{H_2S} = -4$. The potassium-silicate assemblage represented by the pre-Main Stage alteration minerals may be approximated by coexisting annite-microcline on the activity diagram at a log $a_{Fe^{+2}}/a_{H^+}^2 = 2.59$.

Assuming a state of partial equilibrium existed among the pre-Main Stage minerals, the pre-Main Stage assemblage may have exerted an important buffering effect upon the circulating Main Stage fluids. As long as chalcopyrite was present in appreciable quantities, and coexisting with magnetite-hematite-pyrite-biotite and potassium feldspar, the log a_{K^+}/a_{H^+} in the solution was probably buffered between a value of -4.5 to -4.9 and the log $a_{Fe^{+2}}/a_{H^+}^2$ was in the range of 2.52 to 2.95. The buffer capacity may have been outrun near vein structures as chalcopyrite was progressively destroyed during Main Stage activity. At a log $a_{H_2S} = -4.3$ (Fig. 14c) the chalcopyrite field disappears altogether in relatively oxidizing solutions. At these conditions, the dominant species of sulfur is SO_2^{-2} (Meyer and Hemley, 1967). Reaction interval 2, as determined from lithological analysis, consumes ferrous ions to a point where it is possible that the log $a_{Fe^{+2}}/a_{H^+}^2$ in solution diminished as pyrite and bornite coprecipitated. The chalcocite saturation surface is at a log a_{Cu^+}/a_{H^+} of -4.20, very near the triple point pyrite-bornite-covellite-enargite-bornite at a log $(a_{H^+} \cdot a_{As(OH)_4^-}) = -10.7$.

The presence of early pre-Main Stage chalcopyrite in the K-silicate assemblage is interpreted to be of primary importance in buffering the initial Main Stage fluid composition at a relatively high value of log a_{Cu^+}/a_{H^+} near bornite saturation which, fortuitously under the conditions of the Main Stage event, is fairly close to chalcocite saturation and to the stability fields of covellite and enargite. The sequence of coupled irreversible chemical reactions involving alteration, metal leaching, and ultimate ore deposition may be described as induced hypogene sulfide saturation and vein formation related to the initial buffering capacity of the pre-Main Stage assemblage.

Although microscopic methods are used to determine the mineralogy of composite samples, the analytic scale offered in this study is admittedly macroscopic. The physical details of fluid infiltration and diffusion have not been determined and remain interesting problems for future research. Nevertheless, it is possible at this time to make a preliminary interpretation of the overall reaction chemistry deduced in this study in terms of two component fluid transport mechanisms, i.e., infiltration along fractures and diffusion in and out of alteration envelopes surrounding the fractures. The stoichiometric equations listed in Tables 1 through 4 do not specify the sources or sinks of the aqueous species in the reactions as written but only indicate aqueous mobility. Two reactant aqueous species which occur throughout the span of Main Stage reaction monitored by chalcopyrite mass are K^+ and H_4SiO_4. Inspection of oxide component variation with distance from Main Stage veins (Meyer et al., 1968) reveals a variation in K_2O and SiO_2 which may indicate the origin of these aqueous species. Both K_2O and SiO_2 are slightly leached from fresh Butte Quartz Monzonite in the green argillic facies of alteration and are strongly leached in the white argillic facies. There is a superabundance of both these oxides in the sericitic facies. It is therefore possible that K^+ and H_4SiO_4 occur as aqueous reactants in the overall stoichiometric equations due to inward diffusion into the sericitic zone under chemical potential gradients and are not extracted from fluids migrating through Main Stage fractures.

Two aqueous species which maintain a constant reaction position as products in the area studied are Zn^{+2} and Mg^{+2}, resulting, respectively, from sphalerite and biotite destruction. The most likely chemical sink for these elements is the Main Stage fluid itself. The abundance of sphalerite and dolomite in the peripheral parts of the Butte district (Guilbert and Zeihen, 1964) may indicate the final site of deposition of these elements, as well as that of calcium leached initially from plagioclase first by montmorillonite, which underwent replacement by kaolinite and then by sericite. Aqueous species that change reaction position during the various reaction domains, such as H^+, Fe^{+2}, SO_2, O_2, and $H_2As(OH)_5$, do so in step with mineral saturation. Apparently this behavior is a reflection of thermodynamic controls on the fixation of these species in vein-forming minerals such as pyrite and enargite.

A hydrogen ion is a reactant in reaction domain one during simple chalcopyrite leaching and sericitization. However, as large amounts of pyrite precipitate with mirror bornite, the hydrogen ion changes reaction site and becomes a product species, which it remains throughout the duration of the Main Stage event, at least on the western edge of the Butte district. The direct cause of the transition from reactant to product species may be related to oxygenation of hydrothermal fluids by meteoric water and generation of strongly dissociating sulfuric acid which at progressively lower temperatures dissociates readily (Meyer, pers. commun.).

In summary, the overall effects of superposition of Main Stage fluid circulation upon the previously mineralized wall rock in Butte are interpreted as an intimate interchange and redistribution of material, both on a small scale by diffusional processes operating under chemical potential gradients and on a district scale by infiltration through large fracture

TABLE 5. Equilibrium Constants Used to Construct Phase Diagrams

Reaction	log $K_{(1\ bar,\ 350°C)}$	Source
Bornite $Cu_5FeS_4 + 0.5\ H_2O + 6.75\ H^+ = Fe^{+2} + 5\ Cu^+ + 3.875\ H_2S + 0.125\ SO_4^{-2}$	−37.85	1
Chalcopyrite $CuFeS_2 + 0.5\ H_2O + 2.75\ H^+ = Fe^{+2} + Cu^+ + 1.875\ H_2S + 0.125\ SO_4^{-2}$	−11.30	1
Covellite $CuS + 0.5\ H_2O + 0.75\ H^+ = Cu^+ + 0.875\ H_2S + 0.125\ SO_4^{-2}$	8.31	1
Enargite $Cu_3AsS_4 + 5\ H_2O + 1.5\ H^+ = 3\ Cu^+ + As(OH)_4^- + 3.75\ H_2S + 0.25\ SO_4^{-2}$	−40.27	1
Hematite $Fe_2O_3 + 3.5\ H^+ + 0.25\ H_2S = 2\ Fe^{+2} + 0.25\ SO_4^{-2} + 2\ H_2O$	3.13	1
Chalcocite $Cu_2S + 2\ H^+ = 2\ CU^+ + H_2S$	−12.69	2
Magnetite $Fe_3O_4 + 5.5\ H^+ + 0.25\ H_2S = 3\ Fe^{+2} + 0.25\ SO_4^{-2} + 3\ H_2O$	6.08	1
Pyrite $FeS_2 + H_2O + 1.5\ H^+ = Fe^{+2}\ 1.75\ H_2S + 0.255\ SO_4^{-2}$	−7.39	1
Tennantite $Cu_{12}As_4S_{13} + 17\ H_2O + 7.5\ H^+ = 12\ Cu^+ + 4\ As(OH)_4^- + 12.75\ H_2S + 0.25\ SO_4^{-2}$	−152.81	1
Annite-microcline $KFe_3AlSi_3O_{10}(OH)_2 + 6\ H^+ = KAlSi_3O_8 + 4\ H_2O + 3\ Fe^{+2}$	7.76	2

References: 1, Knight (1977); 2, Helgeson (1969).

systems. Involvement of oxygenated meteoric water may not only influence the nature of silicate alteration but also govern directly the final sulfide and oxide assemblages by changing the activities of metal cations relative to hydrogen ions.

Genetic Model of Ore Deposition and Comparison with Other Deposits

As pointed out by Gustafson and Hunt (1975) porphyry copper deposits from various parts of the world differ principally in the degree of development of early versus late mineralization and alteration. The level of intensity of late-stage phenomena may be related to the depth of emplacement of the parent intrusive(s) and the degree of involvement of meteoric ground water (Gustafson and Hunt, 1975; Einaudi, 1977). In comparison, the geology of the multiple-stage deposit at Butte may be described as the superposition and interaction of successive magmatic-hydrothermal episodes. Following intrusion, crystallization, and cooling of the Butte Quartz Monzonite wall rock, Steward-type east-west-striking quartz porphyry dikes intruded the district, introducing, for the first time, ore-forming components. The pre-Main Stage hydrothermal event, perhaps driven by the cooling parent magma of the quartz porphyries, evolved with an initial copper-rich episode and ended with a major event of molybdenum deposition. The resultant fracture-controlled disseminated copper-molybdenum orebody was modified several million years later by the circulation of low-temperature meteoric Main Stage fluids, perhaps driven by a younger intrusive system in the Leonard mine area. Although ore-forming material may have been introduced by the Leonard porphyries (arsenic, perhaps), it is possible that their major role was only as heat engines. It is proposed that the Main Stage vein-forming events represent deep hydrothermal hypogene leaching and enrichment phenomena, analogous in certain respects to the formation of supergene enrichment blankets. The original protore copper grade is envisioned as ultimately determining the metal content and minerology of the late-stage veins, which represent the final redistribution and concentration of elements originally deposited in a lower grade potassium-silicate assemblage. The pre-Main

Stage assemblage might well have functioned as an effective chemical buffer strongly influencing the path of solution compositions during progressive stages of ore deposition and alteration. The pre-Main Stage protore environment may therefore be a necessary condition to the ultimate development of the large high-grade Butte veins.

Acknowledgments

It is a pleasure to acknowledge the inspiration and support of the Anaconda Company staff and members of the faculty of the University of California, Berkeley. Professor Harold Helgeson's pioneering contributions to understanding complex irreversible geochemical processes greatly influenced the approach taken in this study. Professor Charles Meyer has made vitally important scientific discoveries in the Butte district which may ultimately provide for a transition from an era of outmoded selective vein mining to future large-scale production, significantly increasing the life of the Butte mines. The importance of careful rock analyses and petrography to unraveling complex petrologic problems was in a large measure learned from Professor Ian Carmichael. Chief geologist, Richard Miller, Butte Operations, deserves special recognition and gratitude for his leadership of the Anaconda Geological Staff which included the author during a 4-year period. Miller's basic commitment to the necessity of scientific understanding in mineral exploration is an outstanding example of constructive management. Close association with George Burns during the exploration program was a truly rewarding experience. The tragic death of Steven Roberts, fellow student, colleague, and friend for many years, cut short a lifetime of meaningful contribution to economic geology. His special exuberance and creativity greatly influenced all of us working closely with him on the Butte deposit.

Numerous laboratory staff members contributed to this study including Lester Zeihen, Margaret Hocking, Robert Jones, Roy Bloom, Vern Gilman, John Facincani, Linda Pesanti, Mark Pruett, and Paul Kukay. Their efforts are deeply appreciated. Computer services proved to be a necessity in this study and the efforts of Bernard Arvish, Pat Geary, and Tom Cladouhos were invaluable. A word of special gratitude is owed to members of the mine planning and mine operations staff, especially Robert Cox and Robert Moodry, who for a several year period took the time to educate a young mine geologist.

Mark Reed, David Crerar, Marco Einaudi, and Dianne Wolfgram critically read the manuscript, helping to clarify several important points and generally improving the paper. Their thoughtful efforts are much appreciated.

Conversations with Professor George Fisher of Johns Hopkins University provided worthwhile discussions of irreversible thermodynamics.

DEPARTMENT OF GEOLOGY AND GEOPHYSICS
UNIVERSITY OF CALIFORNIA, BERKELEY
BERKELEY, CALIFORNIA 94720
June 26, October 10, 1978

REFERENCES

Anderson, C. A., 1955, Oxidation of copper sulfides and secondary sulfide enrichment: ECON. GEOL., Fiftieth Anniversary Vol., p. 324–340.

Barton, P. B., Bethke, P. M., and Roedder, E., 1977, Environment of ore deposition in the Creede mining district, San Juan Mountains, Colorado: III. Progress toward interpretation of the chemistry of ore-forming fluid for the OH vein: ECON. GEOL., v. 72, p. 1–24.

Brimhall, G. H., 1973, Mineralogy, texture, and chemistry of early wall rock alteration, *in* Miller, R. N., ed., Guidebook for the Butte Field Meeting, Soc. Econ. Geologists: Butte, Montana, The Anaconda Company, p. H-1–H-4.

—— 1976, Analysis of multiple stage porphyry copper mineralization at Butte, Montana [abs.]: Arizona Academy Sci. Jour., v. 11, p. 82.

—— 1977, Early fracture-controlled disseminated mineralization at Butte, Montana: ECON. GEOL., v. 72, p. 37–59.

Burnham, C. W., 1967, Hydrothermal fluids at the magmatic stage, *in* Barnes, H. L., ed., Geochemistry of hydrothermal ore deposits: New York, Holt, Rinehart and Winston, p. 34–76.

Cathles, L. M., 1977, An analysis of the cooling of intrusives by ground-water convection which includes boiling: ECON. GEOL., v. 72, p. 804–826.

Crerar, D. A., and Barnes, H., 1976, Ore solution chemistry. V. Solubilities of chalcopyrite and chalcocite assemblages in hydrothermal solutions at 250° to 350°C: ECON. GEOL., v. 71, p. 772–794.

De Donder, Th., 1928, L'Affinite: Paris, Gauthier-Villars.

De Donder, Th., and Rysselberghe, P. V., 1936, Affinity: Stanford, Calif., Stanford Univ. Press, 142 p.

Einaudi, M. T., 1977, Environment of ore deposition at Cerro de Pasco, Peru: ECON. GEOL., v. 72, p. 893–924.

Ekstrom, T. K., Wirstam, A., and Larson, L. E., 1975, COREMAP—A data system for drill cores and boreholes: ECON. GEOL., v. 70, p. 359–368.

Galehouse, J. S., 1971, Point counting, *in* Carver, R., ed., Procedures in sedimentary petrology: New York, John Wiley and Sons, p. 385–425.

Guilbert, J. M., and Zeihen, L. G., 1964, The mineralogy of the Butte district, Montana: Northwest Mining Association Meeting, Spokane, Washington, Preprint, 20 p.

Gustafson, L. B., and Hunt, J. P., 1975, The porphyry copper deposit at El Salvador, Chile: ECON. GEOL., v. 70, p. 857–912.

Helgeson, H. C., 1968, Evaluation of irreversible reactions in geochemical processes involving minerals and aqueous solutions—I. Thermodynamic relations: Geochim. et Cosmochim. Acta, v. 32, p. 853–877.

—— 1969, Thermodynamics of hydrothermal systems at elevated temperatures and pressures: Am. Jour. Sci., v. 267, p. 729–804.

—— 1970, A chemical and thermodynamic model of ore deposition in hydrothermal systems: Mineralog. Soc. America Spec. Paper 3, p. 155–186.

—— 1971, Kinetics of mass transfer among silicates and aqueous solutions: Geochim. et Cosmochim. Acta, v. 35, p. 421–469.

Helgeson, H. C., Garrels, R. M., and MacKenzie, F. T., 1969, Evaluation of irreversible reactions in geochemical processes involving minerals and aqueous solutions—II. Applications: Geochim. et Cosmochim. Acta, v. 33, p. 455–481.

Helgeson, H. C., Brown, T. H., Nigrini, A., and Jones, T. A., 1970, Calculation of mass transfer in geochemical processes involving aqueous solutions: Geochim. et Cosmochim.. Acta, v. 34, p. 569–592.
Henley, K. J., 1977, Improved heavy-liquid separation at fine-particle sizes: Am. Mineralogist, v. 62, p. 377–381.
Kilinc, I. A., and Burnham, C. W., 1972, Partitioning of chloride between a silicate melt and coexisting aqueous phase from 2 to 8 kilobars: Econ. Geol., v. 67, p. 231–235.
Knight, J. E., 1977, A thermochemical study of alunite, enargite, luzonite, and tennantite deposits: Econ. Geol., v. 72, p. 1321–1336.
Koide, H., and Bhattacharji, S., 1975, Formation of fractures around magmatic intrusions and their role in ore localization: Econ. Geol., v. 70, p. 781–799.
Lacy, W. C., and Hosmer, H. L., 1956, Hydrothermal leaching in Central Peru: Econ. Geol., v. 51, p. 69–79.
Lowell, J. D., and Guilbert, J. M., 1970, Lateral and vertical alteration-mineralization zoning in porphyry ore deposits: Econ. Geol., v. 65, p. 373–408.
Meyer, C., 1965, An early potassic type of alteration at Butte, Montana: Am. Mineralogist, v. 50, p. 1717–1722.
Meyer, C., and Hemley, J. J., 1967, Wall rock alteration, *in* Barnes, H. L., ed., Geochemistry of hydrothermal ore deposits: New York, Holt, Rinehart and Winston, p. 166–235.
Meyer, C., Shea, E. P., Goddard, C. C., Jr., and staff, 1968, Ore deposits at Butte, Montana, *in* Ridge, J. D., ed., Ore deposits of the United States 1933–1967 (Graton-Sales Vol.): New York, Am. Inst. Mining Metall. Petroleum Engineers, v. 2, p. 1363–1416.
Miller, R. N., 1973, Production history of the Butte district and geological function, past and present, *in* Miller, R.N., ed., Guidebook for the Butte Field Meeting, Soc. Econ. Geologists: Butte, Montana, The Anaconda Company, p. F-1–F-11.
Norton, D. L., and Knapp, R., 1977, Transport phenomena in hydrothermal systems: Nature of porosity: Am. Jour. Sci., v. 277, p. 913–936.
Norton, D. L., and Knight, J., 1977, Transport phenomena in hydrothermal systems: cooling plutons: Am. Jour. Sci., v. 277, p. 937–981.
Petruk, W., 1976, The application of quantitative mineralogical analysis of ores to ore dressing: Canadian Inst. Mining Metall. Bull., v. 69, no. 767, March, p. 146–153.
Pillar, C. L. and Drummond, A. D., 1975, Importance of geological data in planning underground ore extraction: Canadian Inst. Mining Metallurgy Bull., v. 68, no. 754, p. 114–116.
Prigogene, I., 1955, Introduction to thermodynamics of irreversible processes: New York, John Wiley and Sons, 119 p.
Proffett, J., 1973, Structure of the Butte district, Montana, *in* Miller, R. N., ed., Guidebook for the Butte Field Meeting, Soc. Econ. Geologists: Butte, Montana, The Anaconda Company, p. G-1–G-12.
Roberts, S. A., 1973, Pervasive early alteration in the Butte District, Montana, *in* Miller, R.N., ed., Guidebook for the Butte Field Meeting, Soc. Econ. Geologists: Butte, Montana, The Anaconda Company, p. HH-1–HH-8.
Roedder, E. W., 1971, Fluid inclusion studies on the porphyry-type ore deposits at Bingham, Utah, Butte, Montana, and Climax, Colorado: Econ. Geol., v. 66, p. 98–120.
Sales, R. H., 1913, Ore deposits at Butte, Montana: AIME Trans., v. 46, p. 4–106.
Sillitoe, R. H., 1972, A plate tectonic model for the origin of porphyry copper deposits: Econ. Geol., v. 67, p. 184–197.
Sutulov, A., 1974, Copper porphyries: Salt Lake City, University of Utah Printing Services, 200 p.
Taylor, H. P., 1974, The application of oxygen and hydrogen isotope studies to problems of hydrothermal alteration and ore deposition: Econ. Geol., v. 69, p. 843–883.
Villas, R. N., and Norton, D., 1977, Irreversible mass transfer between circulating hydrothermal fluids and the Mayflower stock: Econ. Geol., v. 72, p. 1471–1504.
Wallace, S. R., Muncaster, N. K., and staff, 1968, Multiple intrusion and mineralization at Climax, Colorado, *in* Ridge, J. D., ed., Ore deposits of the United States 1933–1967 (Graton-Sales Vol.): New York, Am. Inst. Mining Metall. Petroleum Engineers, v. 1, p. 605–640.
Whitney, J. A., 1975, Vapor generation in a quartz monzonite magma: A synthetic model with application to porphyry copper deposit: Econ. Geol., v. 70, p. 346–358.

APPENDIX

Mineralogical Methods

Wet-screen analyses have been performed on crushed composite samples and show important mineralogic size effects. The volumetric amount of pyrite decreases in smaller size fractions in which chalcocite, bornite, chalcopyrite, and digenite show a higher abundance. Directly related to this mineralogic variation in different size fractions is a progressive in-

TABLE A1. Gravimetric Element Content and Specific Gravity of Heavy Minerals Encountered in This Study

Mineral no.	Symbol	Formula	(M) Cu	Fe	Zn	Pb	Mo	S	As	Ti	Zr	Si	Ca	O	Specific gravity
1	py	FeS_2		46.55				53.45							5.018
2	cc	Cu_2S	79.85					20.15							5.65
3	bn	Cu_5FeS_4	63.31	11.13				25.56							5.07
4	cv	CuS	66.46					33.53							4.682
5	cp	$CuFeS_2$	34.63	30.43				34.94							4.2
6	sl	ZnS			67.09			32.91							4.0
7	en	Cu_3AsS_4	48.41					32.57	19.02						4.45
8	tn	$Cu_{12}As_4S_{13}$	51.56					28.18	20.26						4.642
9	dg	Cu_9S_5	78.11					21.89							5.546
10	mb	MoS_2					59.94	40.06							4.67
11	mt	Fe_3O_4		72.36										27.64	5.175
12	h	Fe_2O_3		69.94										30.06	5.26
13	rt	TiO_2								59.95				40.05	4.37
14	gg	Gangue										46.74		53.26	2.65
15	gn	PbS				86.60		13.40							7.58
16	lm	Limonite		52.27										44.92	3.5
17	Fe	Fe(steel)		99.99											6.2651

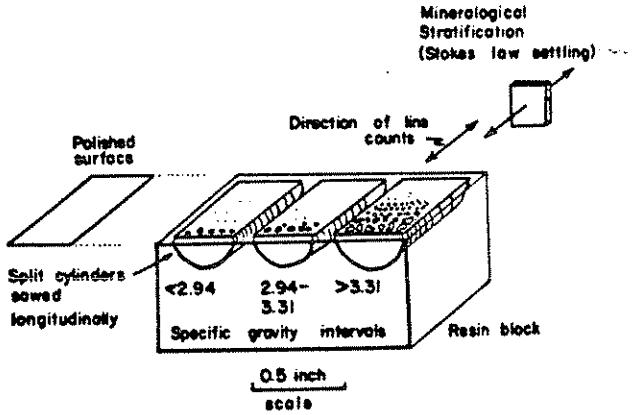

FIG. A1. Split-cylinder geometry showing the direction of integrated line counts using Rosiwal-Shand method of micrometer intercept summation. Direction of line counts is perpendicular to mineral stratification. Interstitial epoxy is not counted.

crease in copper grade in smaller size fractions. It is therefore obvious that methods of heavy mineral separation should not involve a screening step in which finer material is discarded in order to eliminate small grains which are difficult to identify optically. It is necessary to include all of the heavy material in order to retain a representative total sample.

Preparation of resin blocks containing heavy mineral separates has also been investigated. Sulfide mineralogy has been studied as a function of stratigraphic position in liquid resin settling columns with important results. Pyrite and chalcocite are most abundant in the basal settling zones of the resin columns upon solidification. Sphalerite and chalcopyrite are present in much lower quantities in the lower settling zones than on upper horizons.

Two parameters seem to explain the differential mineralogy of heavy mineral layers developed during settling. The specific gravity of the sulfides is obviously an important factor in the settling process within the liquid resin column for grains of comparable size, e.g., chalcocite (sp gr 5.65) is most abundant in upper zones. The average grain size of pyrite (sp gr 5.018) is usually coarser than bornite (sp gr 5.07) and accounts for the high abundance of pyrite in the lower settling zones and increased bornite in upper zones if a settling model obeying Stokes law is invoked. According to such a formulation, the settling velocity is directly proportional to partical density and size. Settling velocity determines the stratigraphic position of sulfides in the resin columns at the time of solidification. Conclusions derived from these simple experiments make it possible to derive a quantitative heavy mineral separation and counting procedure.

Sample Preparation

Material most commonly used for heavy mineral separation consists of composite assay pulps which have been crushed and pulverized to about 50 percent −100 mesh with a sieve opening of 0.0059 inches or 148 microns. As these pulps are necessary for routine assay procedures in exploration, no special effort is required for sample preparation of material to be separated using heavy liquids.

Heavy Mineral Separation

Practice has shown centrifuge techniques to be far superior to separatory funnel methods both in respect to separation time and heavy mineral recovery by reducing extrainment effects of heavy minerals with lighter gangue material. The method derived in this study uses two organic heavy liquids: tetrabromoethane (sp gr 2.94) and methylene iodide (sp gr 3.31). Separation is accomplished by progressive extraction of light, intermediate, and, finally, heavy minerals into three specific gravity intervals (2.94, 2.94-3.31, 3.31).

Forty-gram samples are placed in plastic 250-ml centrifuge bottles which are filled with tetrabromoethane with a specific gravity of 2.94. Following agitation, the bottles are centrifuged at 2,000 rpm for about 1 hour, or until separation produces a clear central layer of fluid containing no suspended material. After centrifuging, floating material with a specific gravity less than 2.94 is removed from sample bottles with an aspirator. Filtration of the light mineral fraction (with Whatman #4 paper) is followed by successive washing with acetone, and heavy liquid is recovered by evaporation of acetone. Light material is dried at about 90°C. The fraction with a specific gravity greater than 2.94 is placed in a necked centrifuge, or Hutton tube, with methylene iodide (sp gr 3.31). Centrifuging at 2,000 rpm usually produces clean separation in about 1 hour. Material floating in the heavy liquid may be removed by placing a closure rod in the Hutton tube down to the point of restriction and decanting into filter paper, followed by washing with acetone. The material with specific gravity greater than 3.31 is removed from the Hutton tube by washing with acetone. Both separations are washed repeatedly with acetone in funnels lined with Whatman #50 filter paper. Oven drying and weighing complete the separation procedure. This separation method is somewhat analogous to that of Henley (1977) in which a Hutton tube is shown but differs in that the present method utilizes no specific gravity gradients in the tubes.

Resin block preparation

A split of each of the specific gravity fractions for an individual sample is placed in small plastic vials

with a metal ball and sufficient resin to fill the vial. After sealing with plastic caps, the vials are placed in a ball mill to assure thorough mixing of sample and resin. The balls are removed, and the vials are allowed to solidify standing in an upright position. Each of the three vials is sawed longitudinally, normal to the mineralogic stratification produced by differential settling velocity, and all three vials are cast side by side in a resin block. The block is ground and polished, resulting in a finished briquette containing representative material of all three specific gravity fractions (Fig. A1). In order to assure good sampling statistics, the maximum amount of sample should be used so that it will bond properly with the resin.

Mineral Identification

The heavy mineral fraction is studied directly by reflected light microscopy. The intermediate and light fractions may also be examined in this way, but it is also possible to prepare thin sections from the resin blocks which are suitable for transmitted light examination of gangue minerals. Electron microprobe examination and point counting of polished surfaces is the ultimate method of study offering both phase identification and mineral composition, but optical methods have so far proven to be satisfactory. In this study, the mineralogy of the silicate material has been determined by alteration facies mapping.

Heavy mineral fractions are counted using a Leitz integrating stage and line-counting procedures (Galehouse, 1971) with the Rosiwal-Shand method. Micrometers record the total length of intercept of individual phases and skip interstitial resin. All counting is done perpendicular to mineral stratification in order to eliminate biased distribution of minerals with different settling velocities (Fig. A1). The maximum number of micrometers on available integrating stages is six, requiring that additional phases be counted using a reticulated ocular. Minerals counted in this fashion require standardization to the same length unit as provided by integrating stage, e.g., objective lens and ocular combination. This method has been found to be much more accurate than normal point counting and requires significantly less time per sample.

Gravimetric Analysis

Conversion of volumetric mineralogic data to a gravimetric basis is performed using average specific gravities of the mineral species (Table A1), showing also the element contents for each mineral used in this study. Small amounts of scrap iron appear in the heavy mineral separate resulting from abrasion of metal parts in the jaw crusher used. Instead of physically removing the scrap iron magnetically, which would also remove pre-Main Stage magnetite, the scrap iron content is determined optically and the resultant gravimetric data is corrected by a calculated removal of the contaminant phase.

Computer Data Reduction

A Fortran computer program was written by the author to reduce the geological and mineralogical data to a useful form allowing graphical determination of the initial pre-Main Stage copper grade. In addition, the total copper grade of each sample is expressed in terms of the contributions of each component sulfide species. Another computer program converts gravimetric data to molar data for a given chemical system size initially containing 1.0 moles of chalcopyrite.